CANCER

Cohesin regulates alternative splicing

Amit K. Singh[1,2], Qingrong Chen[2], Cu Nguyen[2], Daoud Meerzaman[2], Dinah S. Singer[1,2]*

Cohesin, a trimeric complex that establishes sister chromatid cohesion, has additional roles in chromatin organization and transcription. We report that among those roles is the regulation of alternative splicing through direct interactions and in situ colocalization with splicing factors. Degradation of cohesin results in marked changes in splicing, independent of its effects on transcription. Introduction of a single cohesin point mutation in embryonic stem cells alters splicing patterns, demonstrating causality. In primary human acute myeloid leukemia, mutations in cohesin are highly correlated with distinct patterns of alternative splicing. Cohesin also directly interacts with BRD4, another splicing regulator, to generate a pattern of splicing that is distinct from either factor alone, documenting their functional interaction. These findings identify a role for cohesin in regulating alternative splicing in both normal and leukemic cells and provide insights into the role of cohesin mutations in human disease.

INTRODUCTION

Cohesin, a trimolecular ring-shaped complex that encircles chromatin, performs a series of distinct functions throughout the cell cycle. Structurally, it is formed by a heterodimer of structural maintenance of chromosomes (SMC) subunits SMC1 and SMC3, which interlock to generate a hinge domain and an apposed adenosine triphosphatase (ATPase) head, that is bridged by the kleisin subunit RAD21 (*1*). During S, G_2, and early M, cohesin binds DNA in trans and is critical in holding two sister chromatids together (*2*). Hence, cohesin contributes to the regulation of replication and homologous recombination (*3*). Although early studies on cohesin characterized its role during S, G_2, and M, considerable attention has recently focused on cohesin's role during G_1 (*4*–*6*). In contrast to its binding in trans to sister chromatids during S-G_2-M, cohesin associates with chromatin in cis during G_1, where it has two major functions. First, cohesin organizes chromatin into functional domains by mediating the extrusion of chromatin into topologically associated domains or TADs (*7*). Second, cohesin contributes to the regulation of transcription by acting as a scaffold to recruit chromatin remodelers and transcription factors to promoters and by interacting with mediator and stabilizing its interaction with RNA polymerase II (RNAPII) (*1*, *8*). Accordingly, cohesin has been shown to directly facilitate transcriptional activation of *Myc* (*9*).

Cohesin mutations are frequently observed in a variety of different diseases. Among the diseases where cohesin mutations have been found is acute myeloid leukemia (AML), where mutations in cohesin components occur at a frequency of up to 20% (*10*–*12*). AML is frequently associated with large changes in patterns of alternative splicing, where it has been estimated that more than 2000 transcripts undergo altered splicing, with distinct patterns associated with chemosensitivity or resistance (*13*). Splicing in mammalian systems is mediated by the spliceosome, a multi-megadalton complex that assembles on intronic 5′ and 3′ splice sites (*14*). Components of the spliceosome include core U1 to U6 ribonucleoproteins (RNPs) and regulatory cofactors such as fused in sarcoma (FUS), the heterogeneous nuclear RNP (HNRNP), and serine/arginine (SR) protein families (*15*). Although mutations have been observed in both regulatory and core factors of the splicing machinery in 5 to 10% of AML cases (*16*), cohesin mutations seldom occur in the same AML cells as splicing factor mutations (*17*). However, cohesin has recently been found to coimmunoprecipitate with splicing factors (*18*). Despite the critical role of alternative splicing in AML, the role of cohesin has not been examined.

We recently reported that the bromodomain protein, BRD4, contributes to the regulation of alternative splicing both in cells and in vivo (*19*). BRD4 was shown to directly interact with components of the splicing machinery (*19*). BRD4 has many functional parallels with cohesin. Similar to cohesin, BRD4 functions throughout the cell cycle (*20*). During G_2 and M, it functions as a bookmark of active genes (*21*). During G_1, BRD4 is a scaffold for various chromatin remodelers and transcription factors and organizes chromatin into super-enhancers (*22*, *23*). Similar to cohesin, which regulates transcription and undergoes transcription-mediated translocation, BRD4 regulates transcription and travels with the transcription elongation complex (*24*–*30*). Whether cohesin and BRD4 coordinately regulate cotranscriptional or posttranscriptional events has not been examined previously, although the core cohesin subunit, SMC3, has been reported to coimmunoprecipitate in a complex with BRD4 from extracts of cells following γ-irradiation (*31*). The functional parallels between cohesin and BRD4 led us to speculate that cohesin, similar to BRD4, might contribute to the regulation of alternative splicing.

Here, we report that cohesin regulates splicing in cellulo and in vivo. Depletion of cohesin leads to altered patterns of splicing. Introduction of a single point mutation in the cohesin subunit, SMC1, in mouse embryonic stem cells (mESCs), alters both its association with splicing factors and the pattern of splicing. Mechanistically, cohesin interacts with core components of the splicing machinery including U1-70, and the regulatory factors FUS and HNRNPM. Cohesin and BRD4 directly interact and exist in a complex in HCT116 cells where they contribute to a pattern of splicing distinct from that of either factor alone. In primary AML patient samples, cohesin mutations are associated with altered splicing patterns compared with either normal $CD34^+$ cells or AML cells without either cohesin or splicing factor mutations or AML cells with

[1]Experimental Immunology Branch, Center for Cancer Research, Bethesda, MD, USA. [2]Computational Genomics and Bioinformatics Branch, Center for Biomedical Informatics and Information Technology, National Cancer Institute, Bethesda, MD, USA.
*Corresponding author. Email: dinah.singer@nih.gov

splicing factor mutations. Consistent with a direct role of cohesin in alternative splicing in AML, AML-associated cohesin mutations no longer interact with splicing factors. These studies establish a previously unidentified role for cohesin in regulating alternative splicing, either alone or in conjunction with BRD4, and have implications in the characterization of human AML cancer.

RESULTS

Cohesin regulates alternative splicing

The high frequency of both changes in patterns of splicing and in cohesin mutations in AML (*11*, *32*) led us to ask whether cohesin is a regulator of splicing. To address this question, we acutely depleted RAD21/cohesin in human colorectal carcinoma cell line (HCT116 cells) by targeted degradation of RAD21, mediated by an auxin-inducible degron (AID) system (Fig. 1A). In this system, both alleles of RAD21 are fused with a minimal auxin-inducible degradation tag (mAID) (HCT116RmAC cells); short-term auxin treatment leads to nearly complete degradation of RAD21 within 30 min and loss of cohesin function (fig. S1A and movies S1 and S2) (*33*). This acute depletion of RAD21 does not affect the protein levels of other core cohesin subunits SMC1 and SMC3 (fig. S1G) nor does it affect cell viability (fig. S1H). The effect of cohesin depletion on splicing patterns was determined from analyses of RNA sequencing (RNA-seq) data using rMATS 4.0.2 (*34*) for detecting alternative splicing events.

Splicing was significantly affected by depletion of cohesin, relative to the control (Table 1 and fig. S2). Among the five different forms of alternative splicing (Fig. 1B), all the forms were significantly affected, although skipped exon (SE) was the predominant form affected (Table 1). The differential splicing patterns identified by the RNA-seq analysis were validated for representative

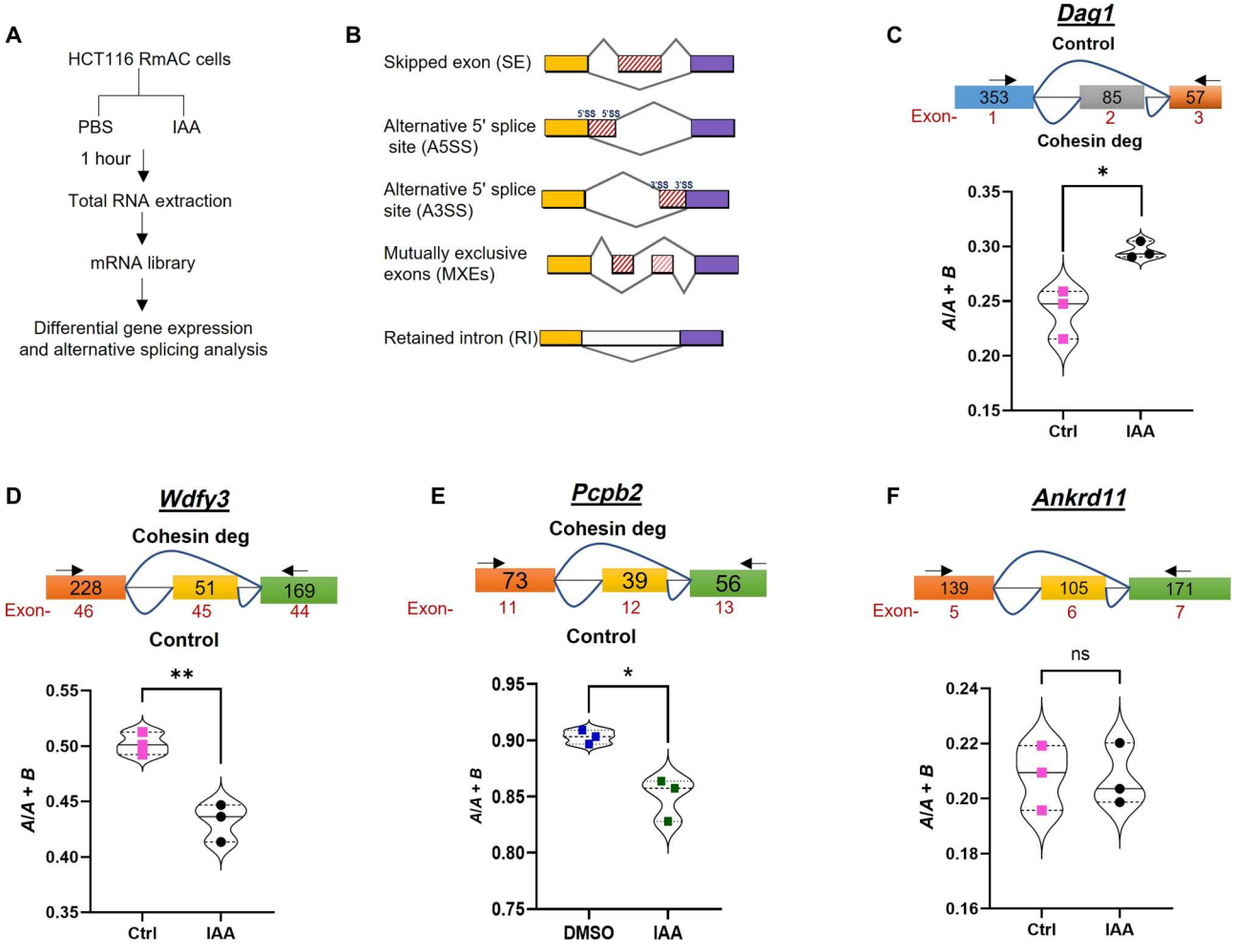

Fig. 1. Cohesin regulates alternative splicing. (**A**) Flowchart showing the experimental protocol, as detailed in Materials and Methods. (**B**) Schematic showing five different classes of alternative splicing events. (**C** to **F**) Top: Schematic representations of genes *Dag1* (C), *Wdfy3* (D), *Pcbp2* (E), and *Ankrd11* (F) focusing on alternatively spliced exons. Colored boxes represent exons, and the horizontal black lines represent the introns; the numbers below the colored boxes refer to the exon number, and numbers inside the boxes represent the length of the exons. The arrowheads depict the approximate reverse transcription polymerase chain reaction (RT-PCR) primer location, and curved lines depict the splicing pattern. (C to E) Bottom: The RT-PCR products derived from total RNA isolated from the cells treated with control or indole-3 acetic acid (IAA) were analyzed on agarose gels as shown in Supplementary Figures. The gels were used to quantify the included (A) and excluded (B) exon transcripts. The violin plots represent the ratios of *A*/*A* + *B* (ratios of included exon transcript/total transcript) used to measure alternative splicing events and represent the data of three independent biological replicates with standard mean deviation. Variables of significance: **P* < 0.05; ***P* < 0.01; and ns, not significant.

Table 1. Cohesin regulates alternative splicing alone or with BRD4. Number of differential splice events/genes following degradation of cohesin or BRD4 or both versus control [false discovery rate (FDR) < 0.05] in HCT116 cells.

	Cohesin depletion		BRD4 depletion		Cohesin + BRD4 depletion	
Splicing type	Differential events	Differentially spliced genes	Differential events	Differentially spliced genes	Differential events	Differentially spliced genes
SE	435	372	1186	958	1206	955
MXE	172	159	273	237	257	221
A5SS	53	50	106	100	119	103
A3SS	44	44	79	78	78	75
RI	12	12	38	38	38	38
Total	716	612	1682	1260	1698	1221

transcripts—*Dag1*, *Wdfy3*, and *Pcbp2*—which were predicted to be affected by cohesin depletion (Fig. 1, C to E). As predicted, depletion of cohesin resulted in a significant increase in *Dag1* exon 2 inclusion (Fig. 1C and fig. S2A). Also as predicted, *Wdfy3* exon 45 and *Pcbp2* exon 12 inclusion were significantly decreased by cohesin depletion (Fig. 1, D and E and fig. S9, E and F). *Wdfy3* exon 45 encodes a segment of the protein that is conserved in rats and humans, although its function is not known (fig. S3A). Notably, exon 12 of *Pcbp2* encodes its nuclear localization signal. The increase in exon 12 exclusion caused by cohesin depletion should result in cytoplasmic mislocalization (fig. S3B). Earlier studies documented that deletion of the nuclear localization signal (NLS) resulted in mislocalization of poly(rC)-binding protein (PCBP2) (*35*). Splicing of the *Ankrd11* transcript was not predicted to be affected by cohesin depletion, and none was detected (Fig. 1F and fig. S2B).

The effects of cohesin depletion on splicing were not due to changes in either steady-state RNA levels or the levels of core and regulatory splicing factors. Degradation of cohesin over the 1-hour treatment period had a minimal effect on total RNA, relative to the control (fig. S4, A to E), and so cannot fully account for the observed effect on splicing. Furthermore, cohesin depletion did not affect the RNA levels of core and regulatory splicing factors (table S1), nor were the protein levels of a subset of splicing factors, the U1-70 component of U1SNRNP core splicing complex, and the regulatory splicing factors FUS and HNRNPM affected in cells depleted of cohesin (fig. S5, A and B). Together, these results provide clear evidence that cohesin contributes to the regulation of the splicing of a subset of transcripts.

Cohesin directly interacts with splicing factors

Two models describe distinct, but not mutually exclusive, mechanisms for the regulation of alternative splicing. The kinetic model proposes that the rate of transcription determines the patterns of cotranscriptional splicing. The recruitment model suggests that alternative splicing is regulated by the association of distinct splicing regulatory factors with exonic junctions (*36*, *37*). Because cohesin has been shown to travel with elongating RNAPII (*24*), we first asked whether the rate of transcription, and hence splicing, is affected by cohesin deletion. We compared the rates of transcription in HCT116 cells with or without cohesin depletion using published precision nuclear run-on sequencing (PRO-seq) data (*38*). Neither RNAPII pausing around the transcription start site (TSS) nor the PRO-seq profile across the metagene body of genes whose transcripts were differentially spliced following cohesin depletion was affected by short-term cohesin depletion (fig. S6A). These results indicate that regulation of alternative splicing by cohesin is not indirect through an effect on transcription.

We next determined whether cohesin regulates splicing through interactions with the splicing machinery. Proximity ligation assays (PLAs) between the RAD21 subunit of cohesin and splicing factors documented in situ colocalization of cohesin with both the U1snRNP component, U1-70, and the regulatory factor, FUS. However, no colocalization of RAD21 with the regulatory component, HNRNPM, or with the nucleolin negative control was observed (Fig. 2, A to C, and fig. S6B).

Extending the finding of cohesin colocalization with splicing factors, metagenomic analysis showed that RAD21 peaks colocalized with FUS binding peak summits across the genome in human embryonic kidney (HEK) 293 cells, whereas acetylation of lysine 27 on histone H3 (H3K27Ac) peaks did not (Fig. 2D, top). In addition, RAD21, but not H3K27Ac, colocalized with FUS across the metagene body (Fig. 2D, bottom).

Furthermore, cohesin and splicing factors associate in vivo, as was demonstrated in coimmunoprecipitation assays in which anti-RAD21 antibody coimmunoprecipitated the spliceosomal component, U1-70, from extracts derived from HCT116 cells (Fig. 2E). Therefore, consistent with its effect on splicing, cohesin is found in a complex with splicing factors, confirming previous reports (*18*).

That cohesin directly interacts with splicing factors was demonstrated in pull-down assays between purified recombinant cohesin subunits, SMC1 and SMC3, and either U1-70 or the regulatory splicing factors, FUS or HNRNPM. Purified rSMC3 was able to efficiently pull-down purified rU1-70. The interaction was unaffected by ribonuclease treatment (Fig. 2F and fig. S6C). rSMC3 also pulled-down purified rFUS, albeit less efficiently than it did U1-70. It did not pull down HNRNPM, consistent with the PLA data (Fig. 2, G and H). Similar to rSMC3, rSMC1 efficiently interacted with rU1-70 and weakly with rFUS (Fig. 2, I and J). Unexpectedly, rSMC1 pulled down rHNRNPM, although colocalization of RAD21 with HNRNPM was not observed by PLA, suggesting that the epitope of one of the two PLA antibodies was not accessible in the PLA (Fig. 2K). These results demonstrate that the cohesin

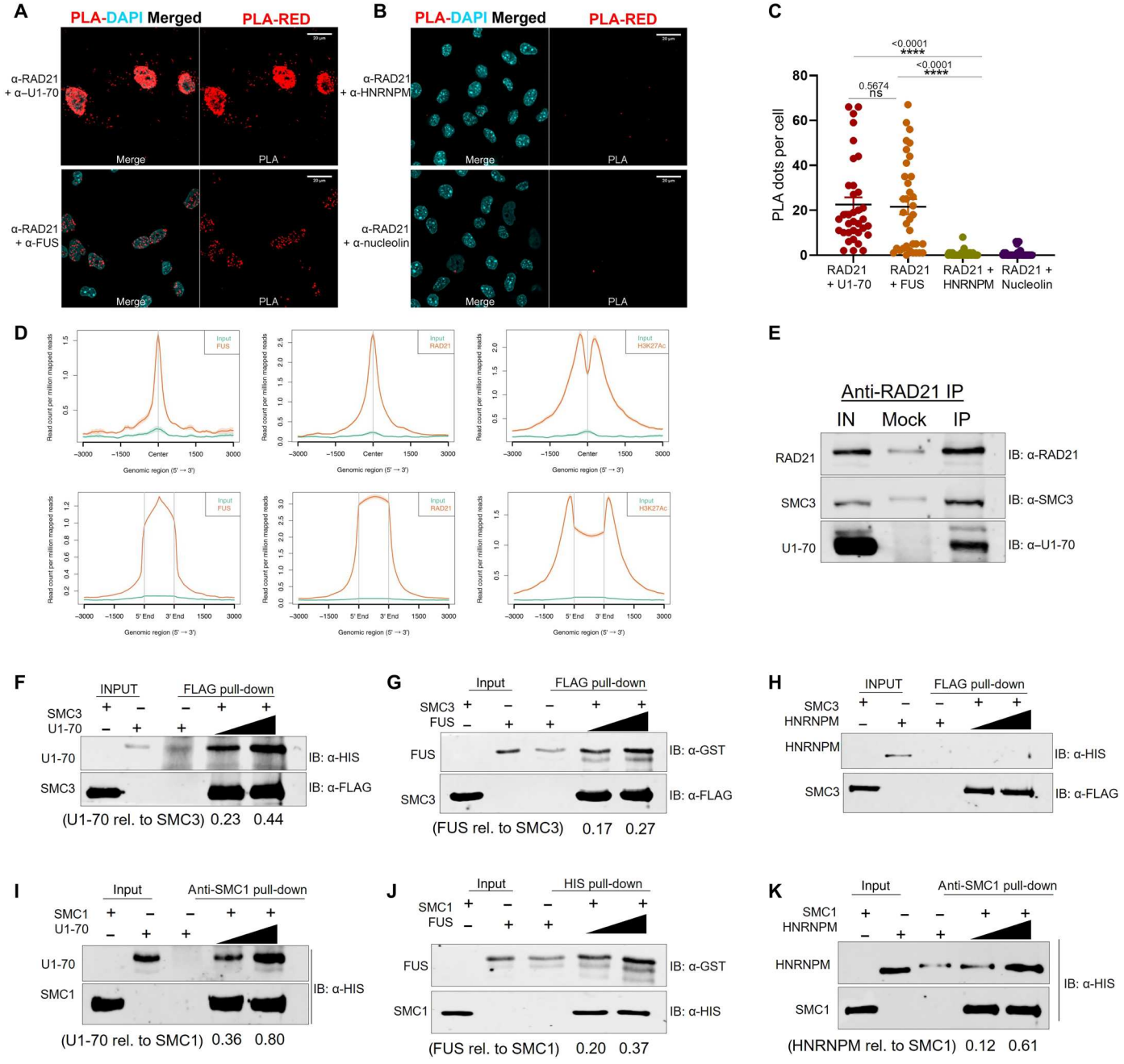

Fig. 2. Cohesin colocalizes and directly interacts with splicing factors. (**A** and **B**) PLAs between anti-RAD21/anti–U1-70, anti-RAD21/anti-FUS (A), anti-RAD21/anti-HNRNPM, and anti-RAD21/anti-nucleolin (B) antibodies. (**C**) Quantification of PLA shown in Fig. 5 (A and B). Statistics were performed with unpaired *t* test with Welch's correction, where $n = 35$ and $^{****}P < 0.0001$ and ns, $P > 0.05$. (**D**) The binding profiles of FUS, RAD21, and H3K27Ac around FUS binding peak summits (top) and FUS binding peaks (bottom). (**E**) Immunoprecipitates from HCT116 whole-cell extracts (WCE) with anti-RAD21 antibody were immunoblotted with the indicated antibodies to RAD21, SMC3, and U1-70. Twenty-five percent of the WCE was used in the input lanes, and immunoglobulin G (IgG; mock) was used as a negative control for the immunoprecipitation (IP) reactions. (**F** to **H**) Immunoblots (IB) showing pull-down analysis of recombinant SMC3 with recombinant U1-70 (F), FUS (G), and HNRNPM (H). rSMC3 (0.90 μg) was incubated with 0.6 and 1.2 μg of U1-70 (molar ratios of 1:2 and 1:4, respectively), 1.6 and 2.6 μg of FUS (molar ratios of 1:3 and 1:5, respectively), and 0.6 and 1.2 μg of HNRNPM (molar ratios of 1:1.5 and 1:3, respectively), followed by pull-down using FLAG beads. Recombinant SMC3 was FLAG tagged; recombinant U1-70 and HNRNPM were HIS tagged, and FUS was glutathione *S*-transferase (GST) tagged. (**I** to **K**) Immunoblots of pull-down assay of recombinant SMC1 (0.92 μg) with 0.6 and 1.2 μg of U1-70 (molar ratios of 1:2 and 1:4, respectively) (I), 1.6 and 2.6 μg of FUS (molar ratios of 1:2 and 1:4, respectively) (J), and 0.6 and 1.2 μg of HNRNPM (molar ratios of 1:1.5 and 1:3, respectively) (K). (I and J) Because SMC1, U1-70, and HNRNPM were HIS tagged, pull-down assays were performed by anti-SMC1 antibody immobilized on protein A Magna beads and (J) pull-down assay of recombinant FUS with SMC1 immobilized on Ni-NTA (nitrilotriacetic acid) beads. DAPI, 4′,6-diamidino-2-phenylindole.

subunits, SMC3 and SMC1, directly interact with splicing factors, providing a mechanism whereby cohesin regulates splicing.

Cohesin and BRD4 co-regulate splicing

In addition to splicing factors, several transcription factors have been reported to affect alternative splicing (*19*, *39*, *40*). We recently reported that the bromodomain protein, BRD4, contributes to the regulation of splicing both in cells and in vivo (*19*). BRD4 was shown to directly interact with components of the splicing machinery (*19*). The present finding that cohesin, similar to BRD4, regulates splicing and directly interacts with splicing factors, led us to ask whether cohesin and BRD4 coordinately regulate splicing. Therefore, we depleted BRD4 in HCT116RmAC cells with the proteolysis-targeted chimera (PROTAC), MZ1, either alone or with indole-3 acetic acid (IAA) to co-deplete RAD21 (Fig. 3A and fig. S1, B to F) (*41*).

Consistent with our previous reports, depletion of BRD4 resulted in a significant change in splicing patterns, as assessed both by the number of differentially spliced events and associated genes (Fig. 3, B and C). [Although depletion of BRD4 alone altered the steady-state RNA profile, relative to the control (fig. S4), those changes did not correlate with changes in alternative splicing.] Unexpectedly, of the differentially spliced events mediated by cohesin depletion alone, only 51 overlapped with those that were affected by BRD4 depletion alone (Fig. 3B). Thus, cohesin contributes to the regulation of splicing of a subset of events that is distinct from BRD4. Even more unexpected, when cohesin and BRD4 were co-depleted, the pattern of splicing differed from the depletion of either alone (Fig. 3, B and C). A total of 1034 splicing events (in 530 genes) were unique to the co-depletion of both cohesin and BRD4. We conclude that cohesin alone, BRD4 alone, and the combination of the two each regulate splicing of distinct subsets of events. All five forms of alternative splicing were significantly affected by the co-depletion of BRD4 and cohesin with SE being the most affected (Table 1 and fig. S7, A and B).

These findings were validated for a few representative transcripts, as described above (Fig. 3, D to G). *Dag1* and *Ankrd11* are examples of transcripts whose splicing is affected only by deletion of cohesin alone or BRD4 alone, respectively. In contrast, *Znf23* is an example of a transcript whose splicing is affected both by deletion of BRD4 alone or in combination with cohesin depletion, although cohesin depletion alone has no effect (Fig. 3F and fig. S7C). A notable case is that of exon 2 of *Qrich1*, which exemplifies a splicing pattern that is unique to the combined deletion of both cohesin and BRD4, where exon inclusion is increased (Fig. 3G and fig. S7D). Thus, cohesin and BRD4 coordinately regulate the patterns of splicing of a subset of transcripts distinct from those regulated by either alone (Fig. 3, D to G).

Stress conditions, such as heat shock, induce both de novo expression of genes and alternative patterns of splicing in cells (*42*). Thus, we next asked whether cohesin and/or BRD4 mediated changes in splicing in HCT116RmAC cells in response to heat shock. Heat shock alone induced large differences in splicing events in control cells (figs. S8 and S9, A to D, and table S2). Heat shock of cohesin-depleted cells induced 2196 unique events relative to cohesin depletion at 37°C. A functional interaction between cohesin and BRD4 was observed following heat shock, where unique splicing events were observed following depletion of the combination of cohesin and BRD4 relative to either alone (fig S9 and table S2). The predicted differential splicing events resulting from heat shock in the absence of cohesin, BRD4, or both were validated for a few representative transcripts (figs. S9, E to G, and S10).

Although heat shock alone markedly affected patterns of total RNA expression relative to the non–heat shock control (fig. S8E), depletion of cohesin did not significantly alter RNA levels in heat-shocked cells (fig. S8, E to G). Notably, changes in steady-state RNA induced by heat shock did not correlate with the observed changes in alternative splicing induced by either BRD4 or cohesin. These results validate the conclusion that cohesin contributes to establishing distinct patterns of alternative splicing independent of changes in transcription and extend the conclusion to the heat shock response.

These results provide further evidence that cohesin, either alone or together with BRD4, contributes to the regulation of splicing of a large number of gene transcripts. The overall pattern of splicing resulting from co-depletion of cohesin and BRD4 is distinct from that of depleting either alone, leading to the conclusion that they coordinately regulate splicing of a subset of transcripts.

Cohesin directly interacts with BRD4

The functional interaction of cohesin and BRD4 in splicing prompted us to ask whether cohesin interacts with BRD4 in vivo or in vitro. To determine whether cohesin and BRD4 are colocalized in cells in situ, their proximity was assessed by PLA. As shown in Fig. 4A, the cohesin subunits RAD21 and SMC3 both colocalized within 30 to 40 nm of BRD4 in the nucleus (Fig. 4B). To further document an interaction in cells, we examined the ability of an anti-BRD4 antibody to coimmunoprecipitate the core cohesin subunits, RAD21 and SMC3, from HCT116 nuclear extract (NE). BRD4 efficiently coimmunoprecipitated both subunits, indicating that BRD4 interacts with the cohesin complex (Fig. 4C, top). The results were confirmed by a reciprocal coimmunoprecipitation (co-IP) using anti-RAD21 antibody, which coimmunoprecipitated both BRD4 and SMC3 (Fig. 4C, bottom). Together, these results demonstrate that cohesin and BRD4 occur in a complex in cells and colocalize in situ (Fig. 4, A to C, and fig. S11A).

To determine whether cohesin and BRD4 directly interact, the ability of purified recombinant cohesin complex to bind to recombinant BRD4 was examined. Using a combination of affinity and size exclusion chromatography, recombinant trimeric cohesin complex was purified to ~90% homogeneity (fig. S11B). In direct pull-down assays, purified recombinant BRD4 efficiently recovered the recombinant cohesin trimeric complex (Fig. 4D). Pull-down assays with BRD4 and purified individual recombinant cohesin core subunits RAD21, SMC3, and SMC1 revealed that BRD4 efficiently interacted with RAD21 and SMC3 but only weakly with SMC1 (Fig. 4, E to G). Although an interaction between the cohesin loading factor, nipped-B-like (NIPBL), has been observed (*43*, *44*), this is the first demonstration that BRD4 directly interacts with the core cohesin complex.

One of the well-established roles of cohesin is to hold sister chromatids together during the period from DNA replication in S phase until mitosis (*2*). BRD4, first identified as a mitotic bookmark, has been shown to associate with mitotic chromatin in several studies (*21*, *45*, *46*). Therefore, we examined whether the interaction of cohesin with BRD4 is cell cycle dependent and restricted to mitosis. The extent of interaction at different stages of the cell

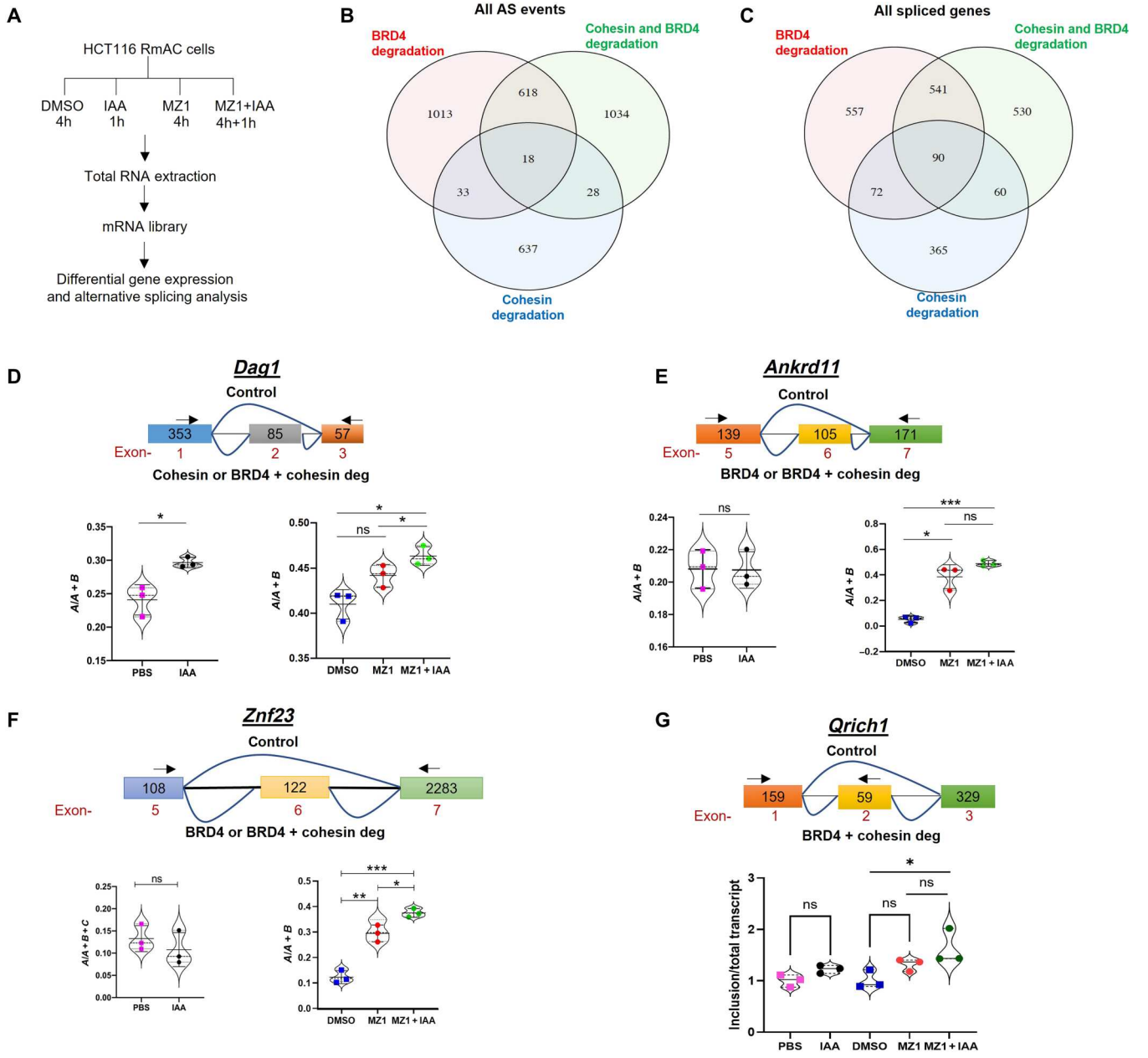

Fig. 3. Cohesin and BRD4 differentially regulate alternative splicing. (**A**) Flowchart showing the experimental scheme, as detailed in Materials and Methods. (**B** and **C**) Venn diagrams showing the relationships among differentially spliced events (B) and alternatively spliced genes (C), resulting from depletion of cohesin alone (blue), BRD4 alone (red), and the combination (green) compared to control. (**D** to **G**) Top: Schematic representations of genes *Dag1* (D), *Ankrd11* (E), *Znf23* (F), and *Qrich1* (G) focusing on alternatively spliced exons. Colored boxes represent exons, and the horizontal black lines represent the introns; the numbers below the colored boxes refer to the exon number, and numbers inside the boxes represent the length of the exons. The arrowheads depict the approximate RT-PCR primer location, and curved lines depict the splicing pattern. (D to F) RT-PCR products derived from total RNA isolated from the cells with different treatments were run on 4% agarose gels containing ethidium bromide (EtBr) (200 ng/ml), followed by quantification of included (A) and excluded (B) exon transcripts. All violin plots represent the ratios of $A/A + B$ (ratios of included exon transcript/total transcript) used to measure alternative splicing events and represent the data of three independent biological replicates with standard mean deviation. (E) Unlike other genes, the splicing of *Qrich1* was validated using quantitative real-time PCR (RT-qPCR). The violin plots summarize the quantitative RT-PCR (RT-qPCR) data with the abundance of *Qrich1* included exon transcripts, resulting from alternative splicing of exons; the data were normalized to total *Qrich1* transcript. Data represent the average of three independent biological replicates with two technical replicates of each RT-qPCR analysis with a standard mean deviation. Variables of significance: $*P < 0.05$, $**P < 0.01$, and $***P < 0.001$. DMSO, dimethyl sulfoxide.

cycle was determined by coimmunoprecipitation from cell extracts following synchronization of cells in early mitosis and release to G_1 (fig. S11C). No difference was seen in the extent of cohesin/BRD4 interaction in either mitotic cells or cells in G_1, relative to asynchronous cells. Therefore, cohesin and BRD4 interact throughout the cell cycle, consistent with their co-regulation of splicing, which occurs mostly during G_1.

Cohesin and BRD4 colocalize at promoters and gene bodies

The finding that cohesin and BRD4 directly interact and coordinately regulate a subset of alternative splicing patterns suggested that they also colocalize on the genome. Although cohesin and BRD4 each have been shown to localize at enhancers (*47*), whether they colocalize more broadly across the genome has not been investigated. Therefore, we analyzed published chromatin immunoprecipitation sequencing (ChIP-seq) datasets for genomic colocalization of cohesin and BRD4 from three different cell lines (*38*, *48*–*52*). Average profiles of SMC1 and RAD21 revealed that these cohesin components colocalized with BRD4 peaks in HCT116 cells, whereas H3K27Ac peaks did not (fig. S12A). SMC1 and SMC3 subunits similarly colocalized with BRD4 peaks in mouse T helper 17 (mT_H17) cells; SMC1, SMC3, and RAD21 also colocalized with BRD4 peaks in mESCs (fig. S12A).

Further analysis revealed a significant colocalization of cohesin with BRD4 at TSS and across BRD4 peaks (fig. S12B). In contrast, cohesin and BRD4 had distinct patterns of localization at typical and super-enhancers (fig. S12C).

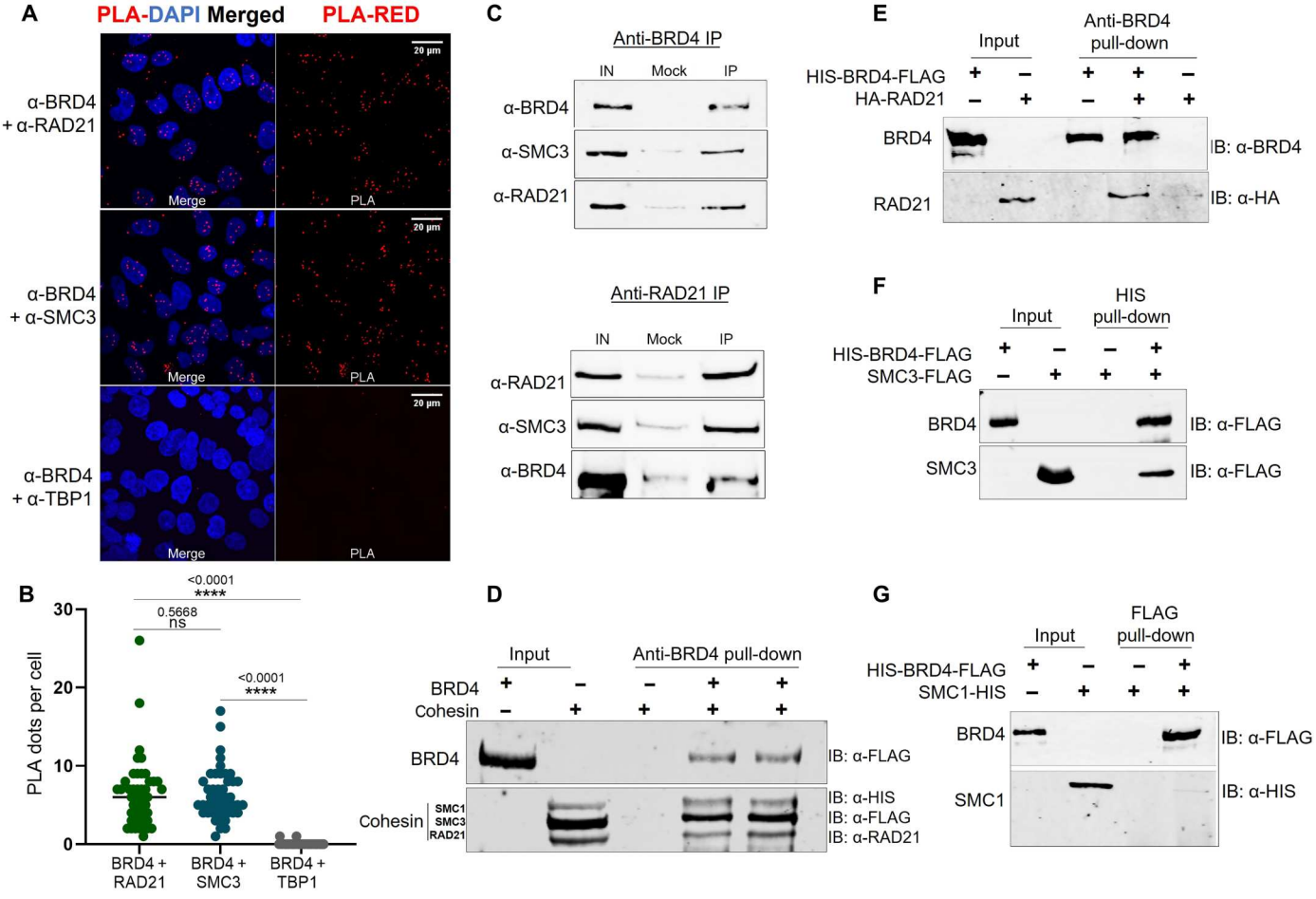

Fig. 4. Cohesin and BRD4 interact in cells and in vitro. (**A**) PLA using anti-BRD4/anti-RAD21 and anti-BRD4/anti-SMC3 antibodies in HeLa cells reveal colocalization between respective proteins. PLA of anti-BRD4/anti-TATAA binding protein 1 (Tbp1) served as a negative control. (**B**) Quantification of PLA shown in (A). Statistics were performed with Unpaired *t* test with Welch's correction, where $n = 47$ and ****$P < 0.0001$ and ns, $P > 0.05$. (**C**) Immunoblots of anti-BRD4 (top) and anti-RAD21 (bottom) immunoprecipitates from HCT116 NEs using the indicated antibodies to BRD4, SMC3, and RAD21. Twenty percent of the NE was used in the input lanes, and IgG (mock) was used as a negative control for the IP reactions. (**D**) Immunoblots showing pull-down analysis of recombinant BRD4 with recombinant cohesin complex. BRD4 (1 μg) was incubated with 2 and 4 μg of cohesin (molar ratio of 1:1 and 1:2, respectively), followed by incubation with anti-BRD4 antibody immobilized on protein A/G Magna beads. Recombinant BRD4 was both HIS and FLAG tagged on the N and C termini, respectively. Recombinant cohesin subunits were tagged as follows: SMC3, C-terminal FLAG; SMC1, C-terminal HIS; and RAD21, N-terminal HA. Blots were sequentially probed with antibodies to FLAG, HIS, and HA. (**E** to **G**) Immunoblots of pull-down assay of 0.3 μg of recombinant RAD21 with 0.50 μg of BRD4 (molar ratio of 1:1) using anti-BRD4 antibody immobilized on protein A/G Magna beads (E), pull-down assay of 0.52 μg of recombinant SMC3 with 0.50 μg of BRD4 (molar ratio of 1:1) immobilized on Ni-NTA beads (F), and pull-down assay of 0.48 μg of recombinant SMC1 with 0.50 μg of BRD4 (molar ratio of 1:1) immobilized on FLAG beads (G).

These results define a previously unknown role for cohesin in regulating alternative splicing, both alone and with BRD4 through direct contacts with splicing machinery components. To determine whether cohesin and BRD4 associate with core splicing machinery independently, we depleted cohesin and BRD4, either alone or together, and examined the proximity of the remaining component to U1-70 by PLA. U1-70 colocalized with both cohesin and BRD4 in control cells. Depletion of BRD4 did not eliminate the cohesin PLA signal with U1-70; conversely, depletion of RAD21 did not eliminate the BRD4 PLA signal with U1-70. Thus, each factor can associate independently with splicing factors (Fig. 5). Unexpectedly, depletion of BRD4 resulted in a significant increase in the colocalization of RAD21 with U1-70 (Fig. 5, A and B, and fig. S13). In contrast, loss of RAD21 did not affect the colocalization of BRD4 and U1-70 (Fig. 5, C and D, and fig. S13).

These results demonstrate that cohesin and BRD4 engage with the splicing machinery. Furthermore, BRD4 appears to compete, in part, with RAD21 for association with spliceosomes. In contrast, the colocalization of BRD4 with splicing factors is not modulated by cohesin. These findings are consistent with the observed distinct

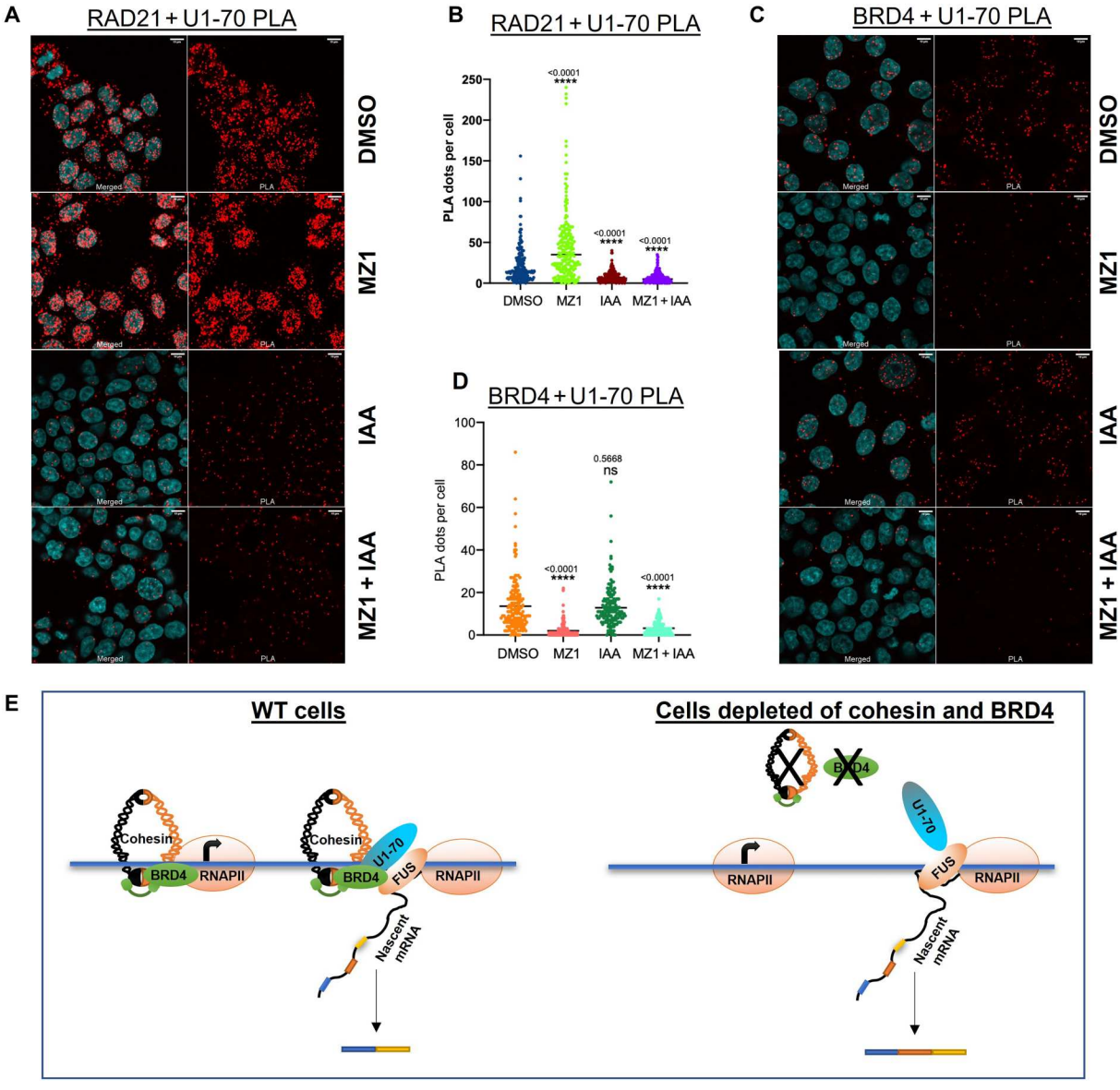

Fig. 5. Proximity of cohesin to U1-70 increases in the absence of BRD4. (**A**) PLAs between anti-RAD21/anti–U1-70 antibodies following the indicated treatment conditions. (**B**) Quantification of PLA shown in (A). Statistics were performed with unpaired *t* test with Welch's correction, where n = ~201 and ****$P < 0.0001$.(**C**) PLAs between anti-BRD4/anti–U1-70 antibodies following the indicated treatment conditions. (**D**) Quantification of PLA shown in (C). Statistics were performed with Unpaired *t* test with Welch's correction, where n = ~175 and ns, $P > 0.05$ and ****$P < 0.0001$. (**E**) Model showing the potential mechanism by which cohesin and BRD4 affect alternative splicing. Both cohesin and BRD4 colocalize with RNAPII at the TSS and in gene bodies. Both interact with a subset of splicing factors where BRD4 is juxtaposed to cohesin in such a manner that it limits the access of cohesin to splicing factors. Overall, this assembly ensures proper splicing. The targeted degradation of cohesin and BRD4 affects the association of splicing factors resulting in changes in alternative splicing. WT, wild-type.

patterns of splicing regulated by cohesin or BRD4 alone and in combination. Together, our findings lead to a model in which cohesin and BRD4 physically and functionally associate with each other and interact with the spliceosome to cotranscriptionally regulate patterns of splicing (Fig. 5E).

Cohesin mutations affect patterns of alternative splicing in patients with AML

Changes in patterns of alternative splicing have been described in a number of cancers. We have previously shown that BRD4 regulates alternative splicing in acute lymphocytic leukemia (*19*). Dysregulated alternative splicing has been linked to molecular pathogenesis in AML where mutations in cohesin occur in up to 20% of cases (*12*, *13*). However, whether there is a correlation between cohesin mutations and changes in patterns of alternative splicing in AML has not been examined. Our findings that depletion of cohesin leads to altered patterns of splicing both in normal growth conditions and in response to heat shock (Fig. 1 and figs. S8 to S10) led us to ask whether cohesin mutations are associated with alternative splicing in primary AML patient samples. We analyzed two independent publicly available RNA-seq datasets from AML patient samples with cohesin mutations [including mutations in core cohesin subunits SMC1, SMC3, and RAD21 and the regulatory subunit stromal antigen 2 (STAG2)], but without splicing factor mutations, and compared the splicing patterns of those samples to those of AML patient samples without either cohesin or splicing factor mutations and to AML patient samples with splicing factor mutations, but no cohesin mutations. The splicing patterns of all of the AML samples were corrected for the overlapping splicing patterns of normal $CD34^+$ peripheral blood lymphocytes (PBLs).

In the analysis of the normal karyotype–AML (NK-AML) cohort, the splicing patterns of a pool of sequencing data from eight patient samples with cohesin, but not splicing factor, mutations were compared with those of a pool of sequencing data from eight AML samples without either cohesin or splicing factor mutations and a pool of sequencing data from three AML samples that had splicing factor mutations but no cohesin mutations (Fig. 6A, and table S3) (*53*). To control for changes in splicing patterns in AML cells that are independent of either cohesin or splicing factor mutations, all samples were compared with, and corrected for, the pooled sequencing data from three $CD34^+$ PBL of healthy controls (Fig. 6A). These analyses revealed unique patterns of splicing associated with cohesin mutations that were not observed in the other datasets. Of particular note, there were significant differences in splicing patterns when the AML samples with cohesin mutations (but no splicing factor mutations) were compared to either those with splicing factor mutations or those without either cohesin or splicing factor mutations.

These findings were confirmed in the analysis of the second, independent dataset, the BEAT-AML cohort (*54*) using a pool of four AML samples with cohesin mutations (but no splicing factor mutations), a pool of eight AML samples with neither cohesin or splicing factor mutations, a pool of four AML samples with splicing factor mutations, but not cohesin mutations, and a pool of eight normal PBL samples (table S3). As observed in the first cohort, there were significant differences in splicing when the AML samples with cohesin mutations were compared to those without cohesin mutations or those with splicing factor, but no cohesin, mutations (Fig. 6B).

These analyses have been confirmed in both datasets using two independent analytical algorithms, rMATS (Fig. 6A) and MAJIQ (fig. S14). Furthermore, in both datasets, while cohesin mutations altered the patterns of splicing, they did not markedly affect the overall distribution of splicing types relative to either AML cells with splicing mutations or those with neither cohesin nor splicing mutations (table S4). On the basis of these analyses, we conclude that cohesin mutations in AML patient samples are highly associated with unique splicing events (Fig. 6 and fig. S14). Note that the genes that are uniquely alternatively spliced in samples with cohesin mutations were enriched for metabolic pathways. Together, these findings provide strong evidence for the role of cohesin in regulating alternative splicing.

A single cohesin point mutation affects alternative splicing

One mechanism by which cohesin could regulate splicing is through its direct interactions with splicing factors, leading to the prediction that the cohesin mutations in AML would no longer interact with splicing factors. To test this prediction, we purified recombinant cohesin subunits with three distinct AML mutations (SMC3 L316P, SMC3 T1174I, and SMC1 K384E) and examined their ability to interact with U1-70. The L316P and T1174I mutations in rSMC3 resulted in the loss of interaction with U1-70 (Fig. 7A). In contrast, the K384E point mutation in SMC1 interacted as efficiently with rU1-70, as did the wild-type (WT) rSMC1 (Fig. 7B). The loss of U1-70 binding by the SMC3 mutants is consistent with the observed changes in splicing in AML patient samples with cohesin mutations and with cohesin-regulating splicing through interactions with the spliceosome.

To further document that cohesin mutations directly affect alternative splicing, we analyzed two clones of mESCs engineered to harbor a single SMC1 point mutation (SMC1a-R586W) that is recurrently observed in patients with AML (*55*). This single cohesin point mutation led to significant changes in splicing (Fig. 7C). Furthermore, as compared to WT cells, two independent SMC1a-R586W mutant clones displayed significantly reduced proximity between U1-70 and RAD21, demonstrating that the SMC1a-R586W mutation affected the association of cohesin with U1-70 (Fig. 7D and fig. S15). Therefore, a single point mutation in SMC1 results in both reduced interactions with splicing factors and altered patterns of splicing.

These results document a novel role for cohesin in the regulation of alternative splicing through its direct interaction with splicing factors. Mutations in the cohesin subunits that lead to reduced interactions result in altered patterns of splicing (Fig. 7E).

DISCUSSION

Alternative splicing is a major mechanism for increasing diversity in gene expression in eukaryotic cells. It has been estimated that 90% of all transcripts can undergo alternative splicing (*56*). Furthermore, aberrant splicing profiles are significantly associated with altered cellular programs in cancers, supporting tumor progression and therapeutic drug resistance in both solid and hematopoietic tumors (*32*). In the present study, we report a splicing mechanism regulated by cohesin, either alone or in combination with BRD4, which mediates distinct patterns of alternative splicing, independent of its effect on transcription or mitosis. We show that cohesin regulates alternative splicing through direct interactions

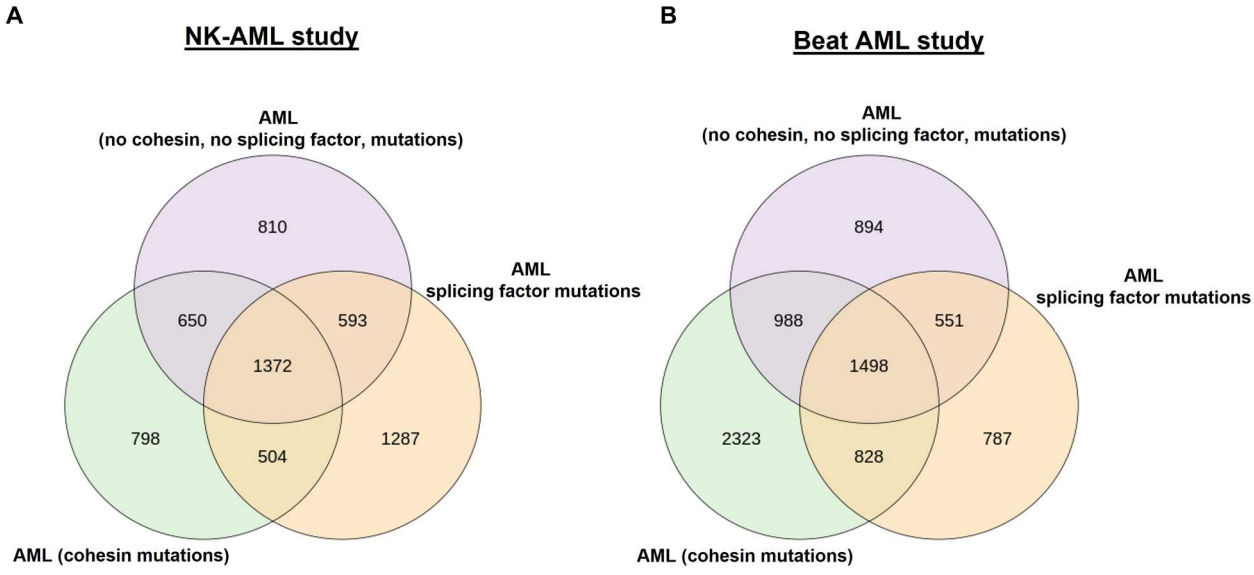

Fig. 6. Cohesin mutations correlate with changes in alternative splicing in patients with AML. (**A** and **B**) Venn diagrams from two different studies, NK-AML (A) and Beat AML (B), showing the relationship of alternatively spliced genes (analyzed by rMATS algorithm) between AML samples with cohesin mutations compared to those with neither cohesin nor splicing factor mutations and those with splicing factor mutations; datasets were compared to $CD34^+$ controls (A) and healthy peripheral blood cells (B) (FDR < 0.05).

and in situ colocalization with splicing factors. Mutations in cohesin that affect those interactions correlate with altered splicing patterns. Unexpectedly, the combination of cohesin and BRD4 together regulate splicing of subsets of transcripts distinct from those regulated by either cohesin or BRD4 alone, indicating that they function cooperatively. Our observation that cohesin is localized across the metagene is consistent with the interpretation that cohesin regulates splicing cotranscriptionally. The functional significance of these observations is reflected in our further finding that cohesin mutations in AML patient samples are highly and uniquely correlated with changes in alternative splicing.

Cohesin, which plays a critical role in sister chromatid alignment during mitosis, also plays critical roles in chromatin organization and gene expression, unrelated to its role in mitosis. Thus, many cohesin mutations paradoxically increase cell proliferation and have been associated with a large number of cancers (*57*). For example, somatic cohesin mutations found in myeloid malignancies do not always correlate with aneuploidy, indicative that cohesin is associated with this cancer by a mechanism other than mitotic. Furthermore, cohesin has been shown to be necessary to sustain neuronal gene expression in postmitotic cells that do not need its cohesion function (*58*).

Somatic mutations in cohesin subunits have been implicated in up to 20% of AML cases, as well as other myeloid malignancies and solid tumors (*10*–*12*). In the present study, we found that AML patient samples with cohesin mutations, but without splicing factor mutations, displayed a distinct set of alternative splicing events that did not occur in either AML cases with splicing factor mutations or without mutations in either cohesin or splicing factors.

Stress responses are associated with many cancers, including AML, to enable cell survival and proliferation. Our finding that cohesin regulates alternative splicing in response to heat shock, another form of stress, is consistent with our finding that cohesin regulates splicing in AML patient cells. We postulate that cohesin may be a general regulator of alternative splicing in response to stress. Together, our findings lead to the hypothesis that cohesin regulation of alternative splicing plays a critical role in maintaining cellular homeostasis and the cohesin mutations that affect splicing are selected for during AML development.

The effect of cohesin on alternative splicing is likely to be cell type specific. Thus, the effects of cohesin on patterns of alternative splicing that occur in AML are distinct from those that we observed in HCT116 cells and ES cells, which are also distinct from each other. In the same way that BRD4 co-regulates splicing with cohesin, we speculate that other factors may similarly co-regulate splicing with cohesin in different cell types.

The mechanism by which cohesin regulates splicing remains to be fully established. It is unlikely to be due to differences in levels of RNA encoding cohesin subunits, which do not differ among the AML subsets. It is also unlikely to be mediated through CCCTC-binding factor (CTCF), which is known to affect splicing through its interactions with polymerase II and other regulatory factors (*59*), as there is no evidence that CTCF directly interacts with splicing factors. It is likely that cohesin regulates splicing through its direct interactions with splicing factors. Our observation that cohesin is localized across the metagene is consistent with the interpretation that cohesin regulates splicing cotranscriptionally. Furthermore, cohesin directly interacts with the spliceosome component, U1-70, and the regulatory splicing factor, FUS. AML-associated mutations in cohesin subunits SMC1 and SMC3 reduce their interactions with U1-70. In addition, introduction of a single point mutation in SMC1 leads to a loss of interaction with splicing factors and changes in alternative splicing in two mESC lines, providing a direct causal link between cohesin and alternative splicing. It has been demonstrated that FUS interacts with the U1snRNP, raising the possibility that cohesin affects this interaction (*60*). We speculate that one mechanism by which cohesin directly regulates

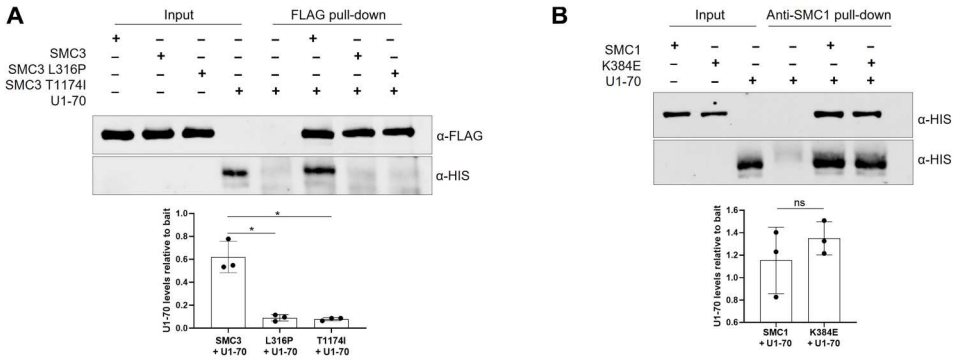

C

Splicing event	Events SMC1 R586W mESC/WT mESC	Genes SMC1 R586W mESC/WT mESC
SE	429	375
MXE	96	87
A5SS	39	36
A3SS	43	42
RI	20	19
Total events/genes	627	500

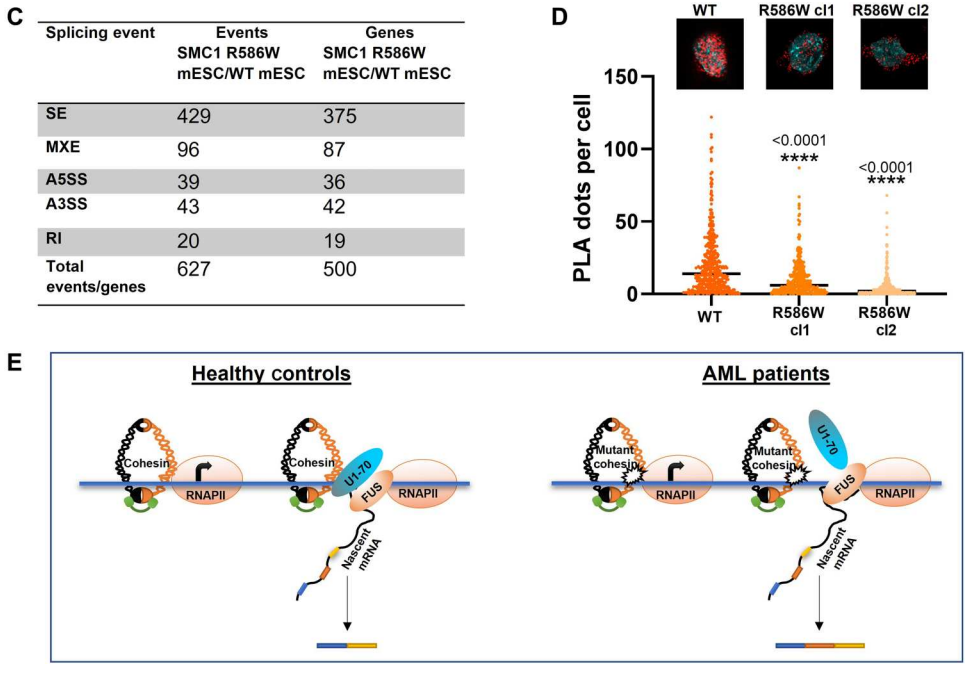

Fig. 7. Cohesin AML mutations affect the interaction with U-70. (**A**) Top: Immunoblots showing pull-down analysis of recombinant WT SMC3 and mutant SMC3 L316P and SMC3 T1174I with recombinant U1-70. SMC3 (0.90 μg) and mutants were incubated with 0.75 μg of U1-70 (molar ratio of 1:2.5) followed by FLAG pull-down. Recombinant SMC3 and mutants were FLAG tagged on the C-terminus. Recombinant U1-70 was HIS tagged. (**B**) Top: Immunoblots showing pull-down analysis of recombinant WT SMC1 and SMC1 K384E with recombinant U1-70. SMC1 (0.92 μg) and mutant were incubated with 0.75 μg of U1-70 (molar ratios of 1:2.5) followed by anti-SMC1 pull-down. Recombinant SMC1, K384E mutant, and U1-70 all were HIS tagged. (A and B) Bottom: Quantitation of respective pull-downs, data of three indivdual replicates with standard mean deviation is plotted; variables of significance *P < 0.05, ns P > 0.05. (**C**) Table showing the number of differential splice events/genes in mESCs with R586W SMC1a mutations compared with WT mESCs (FDR < 0.05). (**D**) Quantification of PLA shown in insets comparing the RAD21-U170 proximity between the two mES SMC1a R586W clones with WT mESCs (see fig. S15B). Statistics were performed with unpaired *t* test with Welch's correction, where $n = 431$ and ****$P < 0.0001$. (**E**) A possible mechanistic model by which cohesin mutations affect alternative splicing in AML. Cohesin colocalizes with RNAPII at the TSS and in gene bodies. Cohesin directly interacts with splicing factors at a subset of genes, ensuring the proper splicing of their transcripts. The cohesin mutations occurring in AML affect cohesin's interaction with splicing factors, resulting in altered patterns of splicing of metabolic pathway genes.

splicing is through modulating the interaction between FUS and U1-70. Although we cannot exclude the possibility that splicing could be indirectly affected if cohesin mutations result in the disruption of cohesin complexes (*11*), both mechanisms may be operative.

In conclusion, we have identified a novel function for cohesin in regulating alternative splicing, both alone and in combination with BRD4. Cohesin mutations observed in AML correlate with changes in patterns of alternative splicing. These findings have potential application to understanding the physiology of AML. Future studies will determine the extent to which cohesin mutations contribute to progression in AML and other cancers.

MATERIALS AND METHODS

Cell lines

Human cell lines

HCT116 and HCT116-RAD21-mAID-mClover cells were cultured in McCoy's 5A medium [American Type Culture Collection (ATCC)] supplemented with 10% fetal bovine serum (FBS; Gemini Bio, 100-106) at 37°C and 7.5% CO_2. HeLa cells were

cultured in Dulbecco's modified Eagle's medium (DMEM; Gibco) supplemented with 10% FBS at 37°C and 7.5% CO_2.

Mouse cell lines

mESC were grown as described previously (*55*). Briefly, WT mESC and both clones harboring SMC1 R586W mutation were cultured in KnockOut DMEM (Thermo Fisher Scientific, 10829-018) supplemented with 15% FBS (Gemini Bio, 100-106), 1× GlutaMAX (Thermo Fisher Scientific, 35050-061), penicillin (100 U/ml) and streptomycin (100 μg/ml; Thermo Fisher Scientific, 15140-122), 1× non-essential amino acids (Thermo Fisher Scientific, 11140-050), 100 μM β-mercaptoethanol (Thermo Fisher Scientific, 21-985-023), and recombinant mouse leukemia inhibitory factor (Sigma-Millipore, ESG1106) at 37°C and 7.5% CO_2.

Insect cells

Drosophila Sf9 cells were grown at 27°C in Sf-900 II insect medium (Thermo Fisher Scientific, 10902088).

Method details

Protein purification

HIS-BRD4-FLAG, SMC3- FLAG, SMC3 L316P-FLAG, and SMC3 T1174I-FLAG were purified using cell extract prepared from Sf9 cells and with the anti-DYKDDDDK G_1 Affinity Resin (GenScript, L00432). FLAG peptide (Sigma-Aldrich, F-3290) was eliminated on a Microcon column (Millipore), and proteins were recovered in 20 mM Hepes (pH 7.8), 150 mM KCl, and 20% (v/v) glycerol followed by preparative fast protein liquid chromatography (FPLC) to remove the traces of contaminants. Similarly, SMC1-HIS, SMC1 K384E-HIS, and hemagglutinin tag (HA)-RAD21 were purified using Sf9 cell extract and with the anti-HIS and anti-HA beads, respectively. The quality of all proteins was assessed on an SDS–polyacrylamide gel electrophoresis (SDS-PAGE), and the purity was evaluated by mass spectrometric analysis [tandem mass spectrometry (MS/MS); NCI Laboratory of Proteomics]. WT trimeric cohesin complex was purified by co-infection of SMC3-FLAG, SMC1-HIS, and HA-RAD21 recombinant baculoviruses into Sf9 cells followed by sequential purification on their respective affinity beads as described in (*61*). The proteins were concentrated on a Microcon column (Millipore) and recovered in 20 mM Hepes (pH 7.8), 150 mM KCl, and 10% (v/v) glycerol. HIS-tagged human HNRNPM (HNRNPM-5432H) and U1-70 (SNRNP70-227H) proteins were purchased from Creative BioMart. Glutathione *S*-transferase (GST)–FUS was purified as described previously (*19*).

Size exclusion chromatography

Recombinant BRD4, SMC3, and SMC1 were further purified using size exclusion chromatography on a Superose 6 Increase 10/300 GL column (manufacturer's exclusion limit, 1000 kDa) on AKTA FPLC (GE Healthcare). The column was pre-equilibrated and run with 20 mM Hepes (pH 7.8), 150 mM KCl, and 5% glycerol at 4°C with a flow rate of 0.3 ml/min, with detection at 280 nm. The column was calibrated with standard molecular weight markers.

Proximity ligation assay

Approximately 10^4 HeLa cells were grown overnight in μ-Slide Angiogenesis (ibidi). PLA was conducted using the Duolink In Situ PLA Kit (Sigma-Aldrich, DUO92101) according to the manufacturer's protocol. The primary antibodies used in Fig. 2 (A and B) and fig. S6B were as follows: rabbit polyclonal anti-RAD21 (Abcam, ab154769), mouse monoclonal anti-FUS immunoglobulin G1 (IgG1; clone 4H11; Santa Cruz Biotechnology, sc-47711), mouse monoclonal anti-HNRNP M1-4 IgG1 (clone 1D8; Santa Cruz Biotechnology, sc-20002), mouse monoclonal anti–U1-70K (clone 9C4.1; EMD Millipore, 05-1588), and mouse monoclonal anti-nucleolin (C23, clone MS-3; Santa Cruz Biotechnology, sc-8031). The primary antibodies used in Fig. 4A and fig. S11A were as follows: mouse monoclonal anti-BRD4 (Sigma-Aldrich, AMAB90841), rabbit polyclonal anti-RAD21 (Abcam, ab154769), rabbit polyclonal anti-SMC3 (Abcam, ab9263), and anti-Tbp1 (Abcam, ab63766). The primary antibodies for RAD21, U1-70, and nucleolin used in Figs. 5 and 7D and figs. S13 and S15 were the same as above; the BRD4 antibody in Fig. 5C used was clone BL-149-2H5 (Bethyl Laboratories, A700-004). Cells were analyzed using either the Zeiss LSM880 Multi-Photon Confocal Microscope or the Yokogawa spinning disk confocal/Nikon Eclipse Ti2 microscope. The signal quantification was done using ImageJ with a custom macro.

NE preparation

HCT116 cells were suspended in lysis buffer [10 mM NaCl, 3 mM $MgCl_2$, 10 mM tris-HCl (pH 7.4), and 0.5% NP-40] with a razor cut pipette tip to avoid shearing, followed by incubation on ice for 5 min. The microfuge tube was centrifuged for 3 s at 13,000 rpm in a 4°C centrifuge to create a nuclear pellet. The supernatant was removed, and the nuclear pellet was resuspended in buffer B (filtered 20 mM Hepes at pH 7.9, 400 mM NaCl, 1 mM EDTA, and 10% glycerol) using approximately 30 μl per 1×10^6 cells. The tube was incubated at 4°C on a rotating wheel for 2 hours. The tube was centrifuged at 4°C for 5 min at 13,000 rpm, and the supernatant containing NE was recovered in a fresh 1.5-ml tube for further experiments.

Coimmunoprecipitation

HCT116 (100 μg) or mESC NE (100 μg) prepared in NE buffer [20 mM Hepes (pH 7.8), 400 mM NaCl, 1 mM EDTA, 10% glycerol, 1× protease inhibitor cocktail (PIC), and 1 mM phenylmethylsulfonyl fluoride] was diluted to 350 μl with NE buffer containing only 100 mM NaCl in a 1.5-ml centrifuge tube. NE was precleared with 20 μl of Protein A/G magnetic beads (Thermo Fisher Scientific, 88803) at 4°C with rotation for an hour. Precleared NE was then incubated with 3 μg of anti-BRD4 rabbit polyclonal (A301-985A50, Bethyl Laboratories), anti-RAD21 rabbit polyclonal (ab154769, Abcam) and anti-SMC3 rabbit polyclonal (Abcam, ab9263), or rabbit IgG antibodies at 4°C with rotation for overnight. Each IP was then incubated with 20 μl of Protein A/G magnetic beads at 4°C with rotation for an hour. Each IP was washed four times with washing buffer [50 mM Hepes (pH 7.8), 200 mM NaCl, 0.5% glycerol, and 0.1% NP-40] at 4°C with rotation for 5 min each. Following the final wash, the residual wash buffer was removed on a magna rack, and the coimmunoprecipitated proteins were eluted by heating in 2× SDS loading buffer at 95°C for 5 min. Immunoblotting was performed following the separation of co-IPs on 8% SDS-PAGE gel, and the proteins were transferred onto a nitrocellulose membrane (GE Healthcare). Following blocking the membrane with 5% skimmed milk in Tris buffered saline with tween 20 (TBST), the blots were incubated with the primary antibodies: anti-BRD4, anti-RAD21, and anti-SMC3 as above and U1-70 (clone 9C4.1; EMD Millipore, 05-1588). Goat anti-rabbit IgG secondary antibody IRDye 800CW (LI-COR Biosciences, 926-32211) and goat anti-mouse IgG secondary antibody IRDye 680RD (LI-COR Biosciences, 926-68070) were used for fluorescence detection of proteins. All immunoblot analyses were performed using the Odyssey infrared scanner. The signal quantification was done using ImageJ software.

Pull-downs

Recombinant cohesin subunit SMC3 was incubated with recombinant splicing factors U1-70, FUS, and HNRNPM for 2 hours at 4°C. FLAG beads (25 μl) were added in all SMC3 pull-down reactions and incubated for overnight at 4°C. All reactions were washed four times with washing buffer [50 mM Hepes (pH 7.8), 200 mM NaCl, 0.5% glycerol, 0.05% NP-40, and 0.05% Tween 20] at 4°C with rotation for 5 min each. All reactions were eluted in 20 μl of wash buffer, and 20 μl of 2× SDS loading buffer was added, and the elutions were heated at 95°C for 5 min before SDS-PAGE and Western blot analysis. SMC1 and FUS pull-down reactions were performed similarly as above except that the 25 μl of HIS beads were used. SMC1/U1-70 and SMC1/HNRNPM pull-down reactions were incubated with 2 μg of anti-SMC1 rabbit polyclonal antibody (Abcam, ab21583) for overnight at 4°C. All reactions were then incubated with 20 μl of Protein A/G Dynabeads at 4°C with rotation for an hour. Washing and elution were performed as above. All pull-downs of U1-70 with recombinant mutant cohesin subunits SMC3-L316P, SMC3-T1174I, and SMC1-K384E were performed as above. Similarly, recombinant BRD4 was incubated with recombinant WT trimeric cohesin complex or individual cohesin subunits SMC1, SMC3, and RAD21 overnight at 4°C. BRD4-cohesin and BRD4-RAD21 pull-downs reactions were incubated with 2 μg of anti-BRD4 rabbit polyclonal antibody (Bethyl Laboratories, A301-985A50). Both reactions were then incubated with 20 μl of Protein A/G Dynabeads at 4°C with rotation for an hour. FLAG beads (25 μl) were added to the BRD4-SMC1 reaction, and 25 μl of anti-HIS beads was added to the BRD4-SMC3 reaction and incubated for 4 hours at 4°C with rotation. Washing and elution was performed as above. All only protein control reactions were carried out similarly. The respective amounts of proteins and their affinity tags are indicated in the figure legends. The following antibodies were used for immunoblotting: anti-HIS mouse monoclonal (Santa Cruz Biotechnology, sc-8036), anti-FLAG mouse monoclonal (GenScript, A00187), anti-GST (Santa Cruz Biotechnology, sc-138), anti-HA mouse monoclonal (GenScript, A01244), anti-BRD4 rabbit polyclonal (Bethyl Laboratories, A301-985A50), and anti-RAD21 rabbit polyclonal (Abcam, ab154769) antibodies. Goat anti-rabbit IgG secondary antibody IRDye 800CW (LI-COR Biosciences, 926-32211) and goat anti-mouse IgG secondary antibody IRDye 680RD (LI-COR Biosciences, 926-68070) were used for fluorescence detection of proteins. All immunoblot analyses were performed using the Odyssey infrared scanner.

Synchronization of cells

The cells were grown to ~50% confluency followed by the addition of 2 mM thymidine, and incubation was continued for 24 hours in a CO_2 incubator. Cells were released from thymidine block by washing using prewarmed 1× phosphate-buffered saline (PBS) two times and once with prewarmed media, fresh DMEM was added, and the incubation was continued for 3 hours. After 3 hours, nocodazole was added at a concentration of 30 ng/ml, and incubation was continued for 14 hours. Prometaphase cells were collected after mitotic shake-off for fluorescence-activated cell sorting (FACS) analysis and cell extract preparation. Shake-off cells were released from prometaphase by washing using prewarmed 1× PBS two times and once with prewarmed media; fresh DMEM was added, and the incubation was continued. Cells were collected after 1-hour (early G_1) and 3-hour (G_1) post-prometaphase release for FACS analysis and whole-cell extract preparation.

Cell culture and targeted depletion of RAD21 and BRD4

HCT116-RAD21-mAID-mClover cells were obtained from the work of Natsume *et al.* (*33*). The cells were cultured in McCoy's 5A medium (ATCC, 30-2007) supplemented with 10% FBS at 37°C and 7.5% CO_2. RAD21 degradation was performed as described by Natsume *et al.* (*33*). For live-cell imaging to monitor RAD21 degradation, the medium was aspirated at $t = 0$ and replaced with either fresh FluoroBrite DMEM (untreated) or FluoroBrite DMEM containing 500 μM IAA. The degradation of RAD21 was monitored on a Nikon Eclipse Ti2 microscope equipped with a stage top incubator to maintain 37°C and 5% CO_2. The images were collected every 30 s for an hour. The data were analyzed using NIS-Elements 4.5 imaging software. The degradation of RAD21 was also confirmed by Western blots. Whole-cell extract (WCE; 50 μg) was separated on an 8% SDS-PAGE followed by immunoblotting using mouse anti-RAD21 rabbit polyclonal (Abcam, ab154769) and rabbit polyclonal anti–β-tubulin (Abcam, ab6046) antibodies. The levels of SMC1 and SMC3 in auxin-treated cells were examined using anti-SMC3 rabbit polyclonal (Abcam, ab9263) and anti-SMC1 rabbit polyclonal antibody (Abcam, ab21583) antibodies.

For the targeted degradation of BRD4, HCT116-RAD21-mAID-mClover cells were cultured as described above followed by replacement of fresh media containing either DMSO or PROTAC MZ1. The different doses of MZ1 ranging from 0.1 to 2 μM were initially used to test the optimal dose for selective degradation of BRD4 as described previously (*41*). The cells were collected after 4 hours of MZ1 treatment followed by preparation of WCE using tissue extraction reagent (Invitrogen) as per the manufacturer's instructions. WCE (50 μg) was separated on an 8% SDS-PAGE followed by immunoblotting using mouse monoclonal anti-BRD4 (Sigma-Aldrich, AMAB90841) rabbit monoclonal anti-BRD2 (Abcam, ab139690), mouse monoclonal anti-BRD3 (Santa Cruz Biotechnology, sc-81202), and rabbit polyclonal anti–β-tubulin (Abcam, ab6046) antibodies.

Cell death assay

The ToxiLight BioAssay Kit (Lonza, catalog no. LT17-217) was used to assess cell death. The assay was performed as per the manufacturer's instructions. This assay quantifies the amount of adenylate kinase (AK) enzyme released into the medium in response to plasma membrane disruption. Briefly, HCT116RmAC cells were treated with PBS or 500 μM IAA for an hour, and the cell supernatant was collected. Cells treated with 1 μM staurosporine for 12 hours were used as a positive control of cell death. Cell supernatant (20 μl) was incubated with 100 μl of AK detection reagent for 5 min, and the luminescence was measured by Synergy HTX multimode plate reader (BioTek).

Heat shock treatment

HCT116-RAD21-mAID-mClover cells were cultured in McCoy's 5A medium (ATCC, 30-2007) supplemented with 10% FBS at 37°C and 7.5% CO_2. RAD21 and BRD4 alone or together were depleted using IAA and MZ1 as described above. Following depletion of proteins, cells were washed twice with 37°C prewarmed media, and then, the cells were replenished with fresh 42°C prewarmed media containing appropriate amounts of IAA and MZ1 alone or

together, and the incubation was continued for an hour in the incubator at 42°C and 7.5% CO_2. For non–heat shock control, the cells were treated similarly except that the cells were replenished with fresh 37°C prewarmed media, and the incubation was continued for an hour at 37°C and 7.5% CO_2.

RNA preparation

RNA was isolated from WT, RAD21 depleted, BRD4 depleted, and BRD4 and RAD21 depleted HCT116 Rad21mAIDmClover cells using the Micro RNeasy Plus Kit (QIAGEN). Libraries were made as described in (*62*).

RNA-seq data analysis

All RNA-seq datasets generated in this study are available at National Center for Biotechnology Information (NCBI) Gene Expression Omnibus (GEO) database (GEO, GSE182960). The SMC1 point mutation RNA-seq dataset was downloaded from GEO as raw fastq files (GSE153576). The datasets used in this study did not include RNA spike-in controls. However, concerns about the lack of spike-in controls should be mitigated by the fact that the analysis of splicing patterns assessed the "isoform proportion" within the same sample, namely, the ratio of spliced transcripts to the total level of transcript ($A/A + B$). For all cell line datasets, RNA-seq reads were aligned to human reference genome hg19 or mouse reference genome mm10 using STAR aligner 2.6.1c. Raw read counts were obtained using htseq-count (*62*) and normalized for further analysis using the built-in normalization algorithms of DESeq2. We used rMATS 4.0.2 (*34*) for detecting alternative splicing events. For rMATS, the significantly differentially spliced events were defined as their false discovery rate (FDR)–adjusted P value of <0.05 and the absolute value of inclusion level difference (IncLevelDifference) > 0.1. The alternative splicing sashimi plots were generated using rmat2sashimiplot (https://github.com/Xinglab/rmats2sashimiplot).

PRO-seq data analysis

The HCT116 PRO-seq dataset was downloaded from GEO as raw fastq files (GSE104334) (*38*). The fastq files from the untreated and treated samples were pooled respectively according to the treatment status. PEPPRO 0.10.0 (http://peppro.databio.org/en/latest/) (*63*) was used to analysis the PRO-seq data, with the polymerase II pausing index results derived from the analysis. The average PRO-seq profile was plotted using ngsplot (https://github.com/shenlab-sinai/ngsplot).

Analysis of AML data

All patient datasets used in the current study are publicly available (*53*, *54*). The NK-AML tumor RNA-seq fastq files were downloaded from dbGAP (dbGaP study accession: phs000159.v11. p5) (*53*). Eight samples with cohesin, but not splicing factor, mutations; eight without either cohesin mutation or splicing factor mutations; and three with only splicing factor mutations were selected on the basis of NK-AML clinical information. Three $CD34^+$ were selected as the normal control. The fastq files were mapped to the human genome GRCh38 GENCODE release 35 using STAR 2.7.8a with the 2-PASS option. The bam files for each category were pooled using samtools merge. The BEAT AML RNA-seq bam files were downloaded from NCI's Genomic Data Commons BEATAML1.0-COHORT study (dbGaP accession: phs001657) mapped to the human genome GRCh38 with the 2-PASS option along with relevant clinical annotations. The patient clinical reference was downloaded from Tyner *et al.* (*54*) (table S5). Four AML samples with cohesin mutations (but no splicing factor mutations), eight AML samples with neither cohesin or splicing factor mutations, four AML samples with splicing factor mutations, and eight normal PBL samples were used. The pooled samples were submitted for alternative-splicing analysis using rMATS 4.1.1 and MAJIQ 2.1 (*64*) with Human GENCODE release 35 gtf annotation and variable-read-length parameter. The significant events were defined as FDR < 0.05 and IncLevelDifference > 0.2 for rMATS. For MAJIQ, the significant local splicing variations (LSVs) were defined as deltaPSI > 0.2 with a confidence greater than 0.95. Pathway analysis was performed using String 11.5 (https://string-db.org) with a filter of confidence of >0.7 and FDR < 0.05.

ChIP-seq data analysis

All ChIP-seq datasets used in this study were downloaded as raw fastq files from public repositories. For HCT116 cells, the BRD4 dataset was downloaded from NCBI GEO (GSE57628); RAD21, SMC1, and H3K27Ac datasets were downloaded from NCBI GEO (GSE104888). For HEK293T cells, the BRD4 dataset was downloaded from NCBI GEO (GSE 51633). FUS dataset was downloaded from NCBI BioProject dataset PRJNA185008. RAD21 and H3K27Ac datasets were downloaded from NCBI GEO (GSE130135). The SMC3 dataset was downloaded from NCBI GEO (GSE44267). The Pol3 dataset was downloaded from NCBI GEO (GSE20309). For T_H17 cells, BRD4 and H3K27Ac datasets were downloaded from NCBI GEO (GSE90788). SMC1 and SMC3 datasets were downloaded from NCBI GEO (GSE63778). For mESCs, the BRD4 dataset was downloaded from NCBI GEO (GSE36561). The RAD21 dataset was downloaded from NCBI GEO (GSE33346). SMC1 and SMC3 datasets were downloaded from NCBI GEO (GSE22562).

For ChIP-seq data analysis, sequencing reads were aligned to human reference genome hg19 or mouse reference genome mm10 using Bowtie2-2.2.3. The duplicated reads were removed, and only uniquely mapped reads were used for peak identification. ChIP-seq peaks were called using MACS 2.1.0 (*65*) with default parameters. The program "ngsplot" was used to generate average profile plots at the specific genomic regions (https://github.com/shenlab-sinai/ngsplot/). The super-enhancers were downloaded from dbSUPER (http://asntech.org/dbsuper), and enhancers were downloaded from EnhancerAtlas 2.0 (http://enhanceratlas.org) for HCT116 cells.

Reverse transcription polymerase chain reaction

cDNA synthesis was performed using SuperScript III First-Strand Synthesis System (Thermo Fisher Scientific, 18080051). Real-time polymerase chain reaction (PCR) reactions were accomplished using the QuantStudio 6 Flex system (Applied Biosystems), in a total volume of 20 μl, using SYBR green-based detection. PCR primer sequences are provided in table S5. PCR amplification conditions comprise an initial cycle of denaturation at 95°C for 3 min, 40 cycles of denaturation at 95°C for 15 s, annealing at optimal temperature for 15 s, and extension at 72°C for 15 s. Fluorescence was measured at the end of the annealing/extension step. Reactions were run in triplicate for each gene, and the specificity of the PCR products was verified by melting curve analysis. The results were

normalized to the total transcript with data belonging to a reference sample (control-treated). Relative expression values were calculated using the 2-ΔΔCT method. The *P* values were calculated using unpaired *t* test to determine the significant difference between treatments. All values obtained were means ± SDs of two technical replicates each in three biological replicates.

Supplementary Materials

This PDF file includes:
Figs. S1 to S15
Tables S1, S2 and S4
Legends for tables S3 and S5
Legends for movies S1 and S2

Other Supplementary Material for this manuscript includes the following:
Tables S3 and S5
Movies S1 and S2

View/request a protocol for this paper from *Bio-protocol*.

REFERENCES AND NOTES

1. S. Rudra, R. V. Skibbens, Cohesin codes–interpreting chromatin architecture and the many facets of cohesin function. *J. Cell Sci.* **126**, 31–41 (2013).
2. D. Dorsett, M. Merkenschlager, Cohesin at active genes: A unifying theme for cohesin and gene expression from model organisms to humans. *Curr. Opin. Cell Biol.* **25**, 327–333 (2013).
3. A. Losada, Cohesin in cancer: Chromosome segregation and beyond. *Nat. Rev. Cancer* **14**, 389–393 (2014).
4. A. Fay, Z. Misulovin, J. Li, C. A. Schaaf, M. Gause, D. S. Gilmour, D. Dorsett, Cohesin selectively binds and regulates genes with paused RNA polymerase. *Curr. Biol.* **21**, 1624–1634 (2011).
5. A. J. Faure, D. Schmidt, S. Watt, P. C. Schwalie, M. D. Wilson, H. Xu, R. G. Ramsay, D. T. Odom, P. Flicek, Cohesin regulates tissue-specific expression by stabilizing highly occupied cis-regulatory modules. *Genome Res.* **22**, 2163–2175 (2012).
6. C. Perea-Resa, L. Wattendorf, S. Marzouk, M. D. Blower, Cohesin: Behind dynamic genome topology and gene expression reprogramming. *Trends Cell Biol.* **31**, 760–773 (2021).
7. Q. Szabo, F. Bantignies, G. Cavalli, Principles of genome folding into topologically associating domains. *Sci. Adv.* **5**, eaaw1668 (2019).
8. A. K. Panigrahi, D. Pati, Higher-order orchestration of hematopoiesis: is cohesin a new player? *Exp. Hematol.* **40**, 967–973 (2012).
9. J. M. Rhodes, F. K. Bentley, C. G. Print, D. Dorsett, Z. Misulovin, E. J. Dickinson, K. E. Crosier, P. S. Crosier, J. A. Horsfield, Positive regulation of c-Myc by cohesin is direct, and evolutionarily conserved. *Dev. Biol.* **344**, 637–649 (2010).
10. B. Leeke, J. Marsman, J. M. O'Sullivan, J. A. Horsfield, Cohesin mutations in myeloid malignancies: Underlying mechanisms. *Exp. Hematol. Oncol.* **3**, 13 (2014).
11. J. B. Fisher, M. McNulty, M. J. Burke, J. D. Crispino, S. Rao, Cohesin mutations in myeloid malignancies. *Trends Cancer* **3**, 282–293 (2017).
12. K. E. Heimbruch, A. E. Meyer, P. Agrawal, A. D. Viny, S. Rao, A cohesive look at leukemogenesis: The cohesin complex and other driving mutations in AML. *Neoplasia* **23**, 337–347 (2021).
13. N. Mehterov, M. Kazakova, Y. Sbirkov, B. Vladimirov, N. Belev, G. Yaneva, K. Todorova, S. Hayrabedyan, V. Sarafian, Alternative RNA splicing—The Trojan Horse of cancer cells in chemotherapy. *Genes (Basel)* **12**, 1085 (2021).
14. C. L. Will, R. Lührmann, Spliceosome structure and function. *Cold Spring Harb. Perspect. Biol.* **3**, a003707 (2011).
15. M. C. Wahl, C. L. Will, R. Lührmann, The spliceosome: Design principles of a dynamic RNP machine. *Cell* **136**, 701–718 (2009).
16. V. Visconte, M. O. Nakashima, H. J. Rogers, Mutations in splicing factor genes in myeloid malignancies: Significance and impact on clinical features. *Cancer (Basel)* **11**, 1844 (2019).
17. C. G. A. R. Network, Genomic and epigenomic landscapes of adult de novo acute myeloid leukemia. *N. Engl. J. Med.* **368**, 2059–2074 (2013).
18. J.-S. Kim, X. He, J. Liu, Z. Duan, T. Kim, J. Gerard, B. Kim, M. M. Pillai, W. S. Lane, W. S. Noble, B. Budnik, T. Waldman, Systematic proteomics of endogenous human cohesin reveals an interaction with diverse splicing factors and RNA-binding proteins required for mitotic progression. *J. Biol. Chem.* **294**, 8760–8772 (2019).
19. S. Uppal, A. Gegonne, Q. Chen, P. S. Thompson, D. Cheng, J. Mu, D. Meerzaman, H. S. Misra, D. S. Singer, The bromodomain protein 4 contributes to the regulation of alternative splicing. *Cell Rep.* **29**, 2450–2460. e5 (2019).
20. B. N. Devaiah, A. Gegonne, D. S. Singer, Bromodomain 4: A cellular Swiss army knife. *J. Leukoc. Biol.* **100**, 679–686 (2016).
21. A. Dey, A. Nishiyama, T. Karpova, J. McNally, K. Ozato, Brd4 marks select genes on mitotic chromatin and directs postmitotic transcription. *Mol. Biol. Cell* **20**, 4899–4909 (2009).
22. J. Loven, H. Hoke, C. Lin, A. Lau, D. Orlando, C. Vakoc, J. Bradner, T. Lee, R. Young, Selective inhibition of tumor oncogenes by disruption of super-enhancers. *Cell* **153**, 320–324 (2013).
23. B. Donati, E. Lorenzini, A. Ciarrocchi, BRD4 and cancer: Going beyond transcriptional regulation. *Mol. Cancer* **17**, 164 (2018).
24. G. A. Busslinger, R. R. Stocsits, P. van der Lelij, E. Axelsson, A. Tedeschi, N. Galjart, J. M. Peters, Cohesin is positioned in mammalian genomes by transcription, CTCF and Wapl. *Nature* **544**, 503–507 (2017).
25. M. S. Borrie, J. S. Campor, H. Joshi, M. R. Gartenberg, Binding, sliding, and function of cohesin during transcriptional activation. *Proc. Natl. Acad. Sci.* **114**, E1062–E1071 (2017).
26. B. N. Devaiah, B. A. Lewis, N. Cherman, M. C. Hewitt, B. K. Albrecht, P. G. Robey, K. Ozato, R. J. Sims III, D. S. Singer, BRD4 is an atypical kinase that phosphorylates serine2 of the RNA polymerase II carboxy-terminal domain. *Proc. Natl. Acad. Sci. U.S.A.* **109**, 6927–6932 (2012).
27. J. D. Weissman et al., The intrinsic kinase activity of BRD4 spans its BD2-B-BID domains. *J. Biol. Chem.* **297**, 101326 (2021).
28. G. E. Winter et al., BET bromodomain proteins function as master transcription elongation factors independent of CDK9 recruitment. *Mol. Cell* **67**, 5–18. e19 (2017).
29. T. Kanno, Y. Kanno, G. LeRoy, E. Campos, H. W. Sun, S. R. Brooks, G. Vahedi, T. D. Heightman, B. A. Garcia, D. Reinberg, U. Siebenlist, J. J. O'Shea, K. Ozato, BRD4 assists elongation of both coding and enhancer RNAs by interacting with acetylated histones. *Nat. Struct. Mol. Biol.* **21**, 1047–1057 (2014).
30. A. Kotekar, A. K. Singh, B. N. Devaiah, BRD4 and MYC: Power couple in transcription and disease. *FEBS J.* (2022); doi: https://doi.org/10.1111/febs.16580.
31. S. R. Floyd, M. E. Pacold, Q. Huang, S. M. Clarke, F. C. Lam, I. G. Cannell, B. D. Bryson, J. Rameseder, M. J. Lee, E. J. Blake, A. Fydrych, R. Ho, B. A. Greenberger, G. C. Chen, A. Maffa, A. M. del Rosario, D. E. Root, A. E. Carpenter, W. C. Hahn, D. M. Sabatini, C. C. Chen, F. M. White, J. E. Bradner, M. B. Yaffe, The bromodomain protein Brd4 insulates chromatin from DNA damage signalling. *Nature* **498**, 246–250 (2013).
32. O. Anczuków, A. R. Krainer, Splicing-factor alterations in cancers. *RNA* **22**, 1285–1301 (2016).
33. T. Natsume, T. Kiyomitsu, Y. Saga, M. T. Kanemaki, Rapid protein depletion in human cells by auxin-inducible degron tagging with short homology donors. *Cell Rep.* **15**, 210–218 (2016).
34. S. Shen, J. W. Park, Z.-x. Lu, L. Lin, M. D. Henry, Y. N. Wu, Q. Zhou, Y. Xing, rMATS: Robust and flexible detection of differential alternative splicing from replicate RNA-Seq data. *Proc. Natl. Acad. Sci. U.S.A.* **111**, E5593–E5601 (2014).
35. A. N. Chkheidze, S. A. Liebhaber, A novel set of nuclear localization signals determine distributions of the αCP RNA-binding proteins. *Mol. Cell. Biol.* **23**, 8405–8415 (2003).
36. I. E. Schor, L. I. Gómez Acuña, A. R. Kornblihtt, in *RNA and Cancer* (Springer, 2013), pp. 1–24.
37. J. A. Hall, P. T. Georgel, *RNA Processing* (IntechOpen, 2011).
38. S. S. P. Rao, S.-C. Huang, B. G. S. Hilaire, J. M. Engreitz, E. M. Perez, K.-R. Kieffer-Kwon, A. L. Sanborn, S. E. Johnstone, G. D. Bascom, I. D. Bochkov, X. Huang, M. S. Shamim, J. Shin, D. Turner, Z. Ye, A. D. Omer, J. T. Robinson, T. Schlick, B. E. Bernstein, R. Casellas, E. S. Lander, E. L. Aide, Cohesin loss eliminates all loop domains. *Cell* **171**, 305–320. e324 (2017).
39. A. Gañez-Zapater, S. D. Mackowiak, Y. Guo, M. Tarbier, A. Jordán-Pla, M. R. Friedländer, N. Visa, A. K. Ö. Farrants, The SWI/SNF subunit BRG1 affects alternative splicing by changing RNA binding factor interactions with nascent RNA. *Mol. Genet. Genomics* **297**, 463–484 (2022).
40. C. Fan, Q. Chen, Q. K. Wang, Functional role of transcriptional factor TBX5 in pre-mRNA splicing and Holt-Oram syndrome via association with SC35. *J. Biol. Chem.* **284**, 25653–25663 (2009).
41. M. Zengerle, K.-H. Chan, A. Ciulli, Selective small molecule induced degradation of the BET bromodomain protein BRD4. *ACS Chem. Biol.* **10**, 1770–1777 (2015).
42. M. Hussong, C. Kaehler, M. Kerick, C. Grimm, A. Franz, B. Timmermann, F. Welzel, J. Isensee, T. Hucho, S. Krobitsch, M. R. Schweiger, The bromodomain protein BRD4 regulates splicing during heat shock. *Nucleic Acids Res.* **45**, 382–394 (2017).
43. G. Olley, M. Ansari, H. Bengani, G. R. Grimes, J. Rhodes, A. von Kriegsheim, A. Blatnik, F. J. Stewart, E. Wakeling, N. Carroll, A. Ross, S.-M. Park; Deciphering Developmental Disorders Study, W. A. Bickmore, M. M. Pradeepa, D. R. FitzPatrick, BRD4 interacts with NIPBL

and BRD4 is mutated in a Cornelia de Lange–like syndrome. *Nat. Genet.* **50**, 329–332 (2018).
44. N. Luna-Peláez, R. March-Díaz, M. Ceballos-Chávez, J. A. Guerrero-Martínez, P. Grazioli, P. García-Gutiérrez, T. Vaccari, V. Massa, J. C. Reyes, M. García-Domínguez, The Cornelia de Lange Syndrome-associated factor NIPBL interacts with BRD4 ET domain for transcription control of a common set of genes. *Cell Death Dis.* **10**, 548 (2019).
45. A. Dey, F. Chitsaz, A. Abbasi, T. Misteli, K. Ozato, The double bromodomain protein Brd4 binds to acetylated chromatin during interphase and mitosis. *Proc. Natl. Acad. Sci. U.S.A.* **100**, 8758–8763 (2003).
46. A. Dey, J. Ellenberg, A. Farina, A. E. Coleman, T. Maruyama, S. Sciortino, J. Lippincott-Schwartz, K. Ozato, A bromodomain protein, MCAP, associates with mitotic chromosomes and affects G2-to-M transition. *Mol. Cell. Biol.* **20**, 6537–6549 (2000).
47. D. Hnisz, B. J. Abraham, T. I. Lee, A. Lau, V. Saint-André, A. A. Sigova, H. A. Hoke, R. A. Young, Super-enhancers in the control of cell identity and disease. *Cell* **155**, 934–947 (2013).
48. L. Baranello, D. Wojtowicz, K. Cui, B. N. Devaiah, H. J. Chung, K. Y. Chan-Salis, R. Guha, K. Wilson, X. Zhang, H. Zhang, J. Piotrowski, C. J. Thomas, D. S. Singer, B. F. Pugh, Y. Pommier, T. M. Przytycka, F. Kouzine, B. A. Lewis, K. Zhao, D. Levens, RNA polymerase II regulates topoisomerase 1 activity to favor efficient transcription. *Cell* **165**, 357–371 (2016).
49. W. Liu, Q. Ma, K. Wong, W. Li, K. Ohgi, J. Zhang, A. K. Aggarwal, M. G. Rosenfeld, Brd4 and JMJD6-associated anti-pause enhancers in regulation of transcriptional pause release. *Cell* **155**, 1581–1595 (2013).
50. N. R. Zemke, D. Gou, A. J. Berk, Dedifferentiation by adenovirus E1A due to inactivation of Hippo pathway effectors YAP and TAZ. *Genes Dev.* **33**, 828–843 (2019).
51. J. C. Schwartz, C. C. Ebmeier, E. R. Podell, J. Heimiller, D. J. Taatjes, T. R. Cech, FUS binds the CTD of RNA polymerase II and regulates its phosphorylation at Ser2. *Genes Dev.* **26**, 2690–2695 (2012).
52. K. L. Cheung, F. Zhang, A. Jaganathan, R. Sharma, Q. Zhang, T. Konuma, T. Shen, J.-Y. Lee, C. Ren, C.-H. Chen, G. Lu, M. R. Olson, W. Zhang, M. H. Kaplan, D. R. Littman, M. J. Walsh, H. Xiong, L. Zeng, M.-M. Zhou, Distinct roles of Brd2 and Brd4 in potentiating the transcriptional program for Th17 cell differentiation. *Mol. Cell* **65**, 1068–1080.e5 (2017).
53. F. Ferraro, C. A. Miller, K. A. Christensen, N. M. Helton, M. O'Laughlin, C. C. Fronick, R. S. Fulton, J. Kohlschmidt, A. K. Eisfeld, C. D. Bloomfield, S. M. Ramakrishnan, R. B. Day, L. D. Wartman, G. L. Uy, J. S. Welch, M. J. Christopher, S. E. Heath, J. D. Baty, M. J. Schuelke, J. E. Payton, D. H. Spencer, M. P. Rettig, D. C. Link, M. J. Walter, P. Westervelt, J. F. DiPersio, T. J. Ley, Immunosuppression and outcomes in adult patients with de novo acute myeloid leukemia with normal karyotypes. *Proc. Natl. Acad. Sci.* **118**, e2116427118 (2021).
54. J. W. Tyner, C. E. Tognon, D. Bottomly, B. Wilmot, S. E. Kurtz, S. L. Savage, N. Long, A. R. Schultz, E. Traer, M. Abel, A. Agarwal, A. Blucher, U. Borate, J. Bryant, R. Burke, A. Carlos, R. Carpenter, J. Carroll, B. H. Chang, C. Coblentz, A. d'Almeida, R. Cook, A. Danilov, K. H. T. Dao, M. Degnin, D. Devine, J. Dibb, D. K. Edwards V, C. A. Eide, I. English, J. Glover, R. Henson, H. Ho, A. Jemal, K. Johnson, R. Johnson, B. Junio, A. Kaempf, J. Leonard, C. Lin, S. Q. Liu, P. Lo, M. M. Loriaux, S. Luty, T. Macey, J. MacManiman, J. Martinez, M. Mori, D. Nelson, C. Nichols, J. Peters, J. Ramsdill, A. Rofelty, R. Schuff, R. Searles, E. Segerdell, R. L. Smith, S. E. Spurgeon, T. Sweeney, A. Thapa, C. Visser, J. Wagner, K. Watanabe-Smith, K. Werth, J. Wolf, L. White, A. Yates, H. Zhang, C. R. Cogle, R. H. Collins, D. C. Connolly, M. W. Deininger, L. Drusbosky, C. S. Hourigan, C. T. Jordan, P. Kropf, T. L. Lin, M. E. Martinez, B. C. Medeiros, R. R. Pallapati, D. A. Pollyea, R. T. Swords, J. M. Watts, S. J. Weir, D. L. Wiest, R. M. Winters, S. K. McWeeney, B. J. Druker, Functional genomic landscape of acute myeloid leukaemia. *Nature* **562**, 526–531 (2018).
55. Z. M. Carico, H. C. Stefan, M. Justice, A. Yimit, J. M. Dowen, A cohesin cancer mutation reveals a role for the hinge domain in genome organization and gene expression. *PLOS Genet.* **17**, e1009435 (2021).
56. F. E. Baralle, J. Giudice, Alternative splicing as a regulator of development and tissue identity. *Nat. Rev. Mol. Cell Biol.* **18**, 437–451 (2017).
57. T. Waldman, Emerging themes in cohesin cancer biology. *Nat. Rev. Cancer* **20**, 504–515 (2020).
58. F. D. Weiss, L. Calderon, Y.-F. Wang, R. Georgieva, Y. Guo, N. Cvetesic, M. Kaur, G. Dharmalingam, I. D. Krantz, B. Lenhard, A. G. Fisher, M. Merkenschlager, Neuronal genes deregulated in Cornelia de Lange Syndrome respond to removal and re-expression of cohesin. *Nat. Commun.* **12**, 2919 (2021).
59. A. B. Alharbi, U. Schmitz, C. G. Bailey, J. E. Rasko, CTCF as a regulator of alternative splicing: New tricks for an old player. *Nucleic Acids Res.* **49**, 7825–7838 (2021).
60. Y. Yu, R. Reed, FUS functions in coupling transcription to splicing by mediating an interaction between RNAP II and U1 snRNP. *Proc. Natl. Acad. Sci. U.S.A.* **112**, 8608–8613 (2015).
61. R. Ladurner, V. Bhaskara, P. J. Huis in 't Veld, I. F. Davidson, E. Kreidl, G. Petzold, J. M. Peters, Cohesin's ATPase activity couples cohesin loading onto DNA with Smc3 acetylation. *Curr. Biol.* **24**, 2228–2237 (2014).
62. A. Gegonne, Q. R. Chen, A. Dey, R. Etzensperger, X. Tai, A. Singer, D. Meerzaman, K. Ozato, D. S. Singer, Immature CD8 single-positive thymocytes are a molecularly distinct subpopulation, selectively dependent on BRD4 for their differentiation. *Cell Rep.* **24**, 117–129 (2018).
63. J. P. Smith, A. B. Dutta, K. M. Sathyan, M. J. Guertin, N. C. Sheffield, PEPPRO: Quality control and processing of nascent RNA profiling data. *Genome Biol.* **22**, 155 (2021).
64. J. Vaquero-Garcia, A. Barrera, M. R. Gazzara, J. González-Vallinas, N. F. Lahens, J. B. Hogenesch, K. W. Lynch, Y. Barash, A new view of transcriptome complexity and regulation through the lens of local splicing variations. *eLife* **5**, e11752 (2016).
65. Y. Zhang, T. Liu, C. A. Meyer, J. Eeckhoute, D. S. Johnson, B. E. Bernstein, C. Nusbaum, R. M. Myers, M. Brown, W. Li, X. S. Liu, Model-based analysis of ChIP-Seq (MACS). *Genome Biol.* **9**, R137 (2008).

Acknowledgments: We are grateful to J. Dowen for providing the mESC lines. We thank T. Ley, F. Ferraro, and C. Miller for helpful discussions, suggestions, and sharing of AML data. We thank J. M. Peters for providing the HIS-SMC1, FLAG-SMC3, and RAD21-HA pFAST-Bac1 plasmids. We also thank M. Kanemaki for providing the HCT116 RmAC cell line. We acknowledge A. Roy, R. Sen, S. Uppal, M. Walter, and I. Bag for critical reading of the manuscript. We also acknowledge the CCR genomics core for routine sequencing of plasmid constructs. We also thank the members of the Singer laboratory for helpful discussions throughout these studies. This study used the high-performance computational capabilities of the Biowulf Linux cluster at the NIH (http://biowulf.nih.gov). **Funding:** This work was supported by the Intramural Research Program of the NIH, National Cancer Institute, Center for Cancer Research. **Author contributions:** A.K.S. and D.S.S. conceptualized the study. A.K.S. performed the experiments. A.K.S., Q.C., C.N., D.M., and D.S.S. analyzed the data. A.K.S. and D.S.S. wrote the manuscript with editing by Q.C. and D.M. **Competing interests:** The authors declare that they have no competing interests. **Data and materials availability:** All generated data are available in the main text or Supplementary Tables. The RNA-seq data generated in this study are deposited under GEO accession number GSE182960. Materials generated in this study are available upon request. SMC1a R586W mESC lines can be provided by J. Dowen (jilldowen@unc.edu); HIS-SMC1, FLAG-SMC3, and RAD21-HA pFAST-Bac1 plasmids can be provided by J. M. Peters (peters@imp.ac.at); HCT116 RmAC cell line can be provided by M. Kanemaki (mkanemak@nig.ac.jp). All pending scientific review and a completed material transfer agreement.

Submitted 12 August 2022
Accepted 26 January 2023
Published 1 March 2023
10.1126/sciadv.ade3876